scientific reports

Check for updates

OPEN

The oleaginous yeast *Cutaneotrichosporon oleaginosum* modifies corn stover alkali lignin

Austin Gluth[1,2], Yunqiao Pu[3], Dehong Hu[2], Xiaowen Chen[4], Zachary Johnson[1,2], Xiaolu Li[2], Arthur J. Ragauskas[3], Wei-Jun Qian[2], Tong Zhang[2] & Bin Yang[1,2]✉

The current paradigm in synthetic biology for lignin bioconversion platforms includes primarily bacteria and filamentous fungi. Yeast are notoriously understudied for their role in lignin degradation and utilization, despite their ubiquity in saprophytic microbial communities. A few publications report lignin-modifying yeasts, but investigations to date have relied on model aromatic compounds or lignin-containing substrates replete with other carbon sources. In this work, we use a suite of analytical tools to evaluate interactions between corn stover-extracted lignin and the oleaginous yeast *Cutaneotrichosporon oleaginosum*. Notably, 2D-NMR analysis showed a significant decrease in the H-lignin component as well as resinol (β-β) and phenylcoumaran (β-5) linkages. Using super-resolution fluorescence microscopy, we demonstrated that this yeast may uptake polymeric lignin and/or undertakes interactions at the cellular envelope. To explore mechanisms of lignin modification, transport, and aromatics catabolism, extensive secretomics and proteomics analyses were conducted. Compared to carbon-limited glucose and "No Carbon" controls, several putative laccases, quinone reductases, superoxide dismutases, and glyoxal/oxalate oxidases were upregulated in the lignin condition. Excitingly, two ferric reductases and an oxalate exchanger were only observed in the lignin condition. These results indicate that *C. oleaginosum* may perform extracellular quinone redox cycling to generate lignin-modifying reactive oxygen species. These findings enhance our understanding of yeast-lignin interactions and provide valuable insights for validation studies and metabolic engineering.

Lignin constitutes a complex and diverse biopolymer, and, importantly, it is the largest renewable source of aromatics. As much as 40% of the energy density of lignocellulosic biomass is found in lignin, and it has a higher carbon content than carbohydrates: 68 wt% for the lignin derivative guaiacyl vs. 44% for cellulose based on glucose[1]. Bacteria and filamentous fungi are prime candidates for leveraging this rich carbon source given their ligninolytic capabilities[2–5]. In general these microorganisms degrade lignin using oxidoreductases such as laccases and peroxidases as well as other redox-active molecules[6–8]. Compared to filamentous fungi, bacteria such as *Pseudomonas putida* have higher growth rates and are amenable to genetic manipulation; nevertheless, white rot fungi like *Phanerchaete chrysosporium* are superior lignin degraders[9]. In contrast the potential of yeasts (particularly basidiomycetes) as biocatalysts for lignin valorization and their roles in lignin-containing microbial niches has rarely been investigated. As a result, a clarity regarding their ability to degrade (or at least modify) lignin and what enzymes may functionally confer these capabilities is lacking[10].

Though scarce, there are reports of basidiomycete yeasts (and one ascomycete) with enzymatic activities against lignin as the major carbon source. These include species of the genera *Rhodotorula*, *Geotrichum*, *Tausonia*, and *Cutaneotrichosporon*[11–14]. Laccase, manganese peroxidase, and lignin peroxidase activities have been observed in yeasts—some of which display the oleaginous phenotype under nutrient-limiting conditions[14–17]. Oleaginous yeast accumulates lipids and are promising candidates for sustainable synthesis of palm oil substitutes, lubricants, plastics, and fuels[18–21]. Of these yeasts, *Cutaneotrichosporon oleaginosum* (formerly known as *Cryptococcus curvatus* and later *Trichosporon oleaginosus*) is poised for lignin valorization because it can accumulate lipids using the monoaromatic resorcinol[22–24]. However, it is unclear if this yeast can degrade lignin, and what enzymatic mechanisms are involved both extra- and intracellularly. A recent functional genomics analysis of *C. oleaginosum* cultivated on alkali-pretreated corn stover has expanded our knowledge of

[1]Bioproducts, Sciences, and Engineering Laboratory, Department of Biological Systems Engineering, Washington State University, Richland, WA, USA. [2]Earth & Biological Sciences, Pacific Northwest National Laboratory, Richland, WA, USA. [3]Biosciences Division, Oak Ridge National Laboratory, Oak Ridge, TN, USA. [4]Biosciences Center, National Renewable Energy Laboratory, Golden, CO, USA. ✉email: bin.yang@wsu.edu

yeast aromatics catabolism but again raises questions about its ligninolytic abilities due to ambiguous results from K-lignin analysis, NMR spectroscopy, and enzymatic activity assays[14,25]. For instance, a decrease in the acetyl groups of the alkali-pretreated corn stover was observed whereas no changes to the (hemi)cellulose fractions were reported, raising the possibility that lignin in the black liquor was blocked[25].

The hydrolysate derived from dilute-alkali corn stover pretreatment contains numerous accessible carbon sources apart from lignin: monomeric sugars, oligosaccharides, organic acids, and monoaromatics[26,27]. Other studies have used modified (Kraft) lignin in the presence of glucose, which obfuscates secretomics results[28]. We cultivated *C. oleaginosum* on lignin purified from alkali-pretreated corn stover to directly evaluate lignin degradation/modification[29]. We hypothesize that the proposed yeast secretes redox-active, lignin-modifying enzymes during carbon limitation, and that liberated aromatics and polymeric lignin are proximally transported into the cell. Our 2D-NMR results demonstrate decreases in the H- and G-lignin motifs and relative changes to bonding in the lignin structure. Our preliminary fluorescence microscopy results suggest cellular uptake of polymeric lignin. Passive and active transport of lignin-derived aromatics has been studied, but there is a dearth of information regarding lignin fragments[30–33]. *Saccharomyces cerevisiae* can uptake nanoparticles of polyaromatic polystyrene, which indirectly supports yeast lignin uptake[34]. Our fluorescence microscopy approach which harnesses the native fluorescent properties of lignin may corroborate this[35,36]. Finally, we developed a comprehensive secretomics and proteomics workflow to study the expressed metabolism of *C. oleaginosum*, thereby pinpointing putative enzymes for lignin modification as well as transport and utilization of lignin-derived aromatics. This comprehensive work provides targets for functional evaluation and additional impetus for developing basidiomycete yeasts as chassis for lignin valorization.

Results and discussion

Cultivation on alkali lignin is reminiscent of the "No Carbon" condition

A multifaceted approach was employed to study the cultivation of *C. oleaginosum* on alkali lignin and is summarized in Fig. 1. Lignin from dilute alkali-pretreated corn stover was extracted with successive acid-base

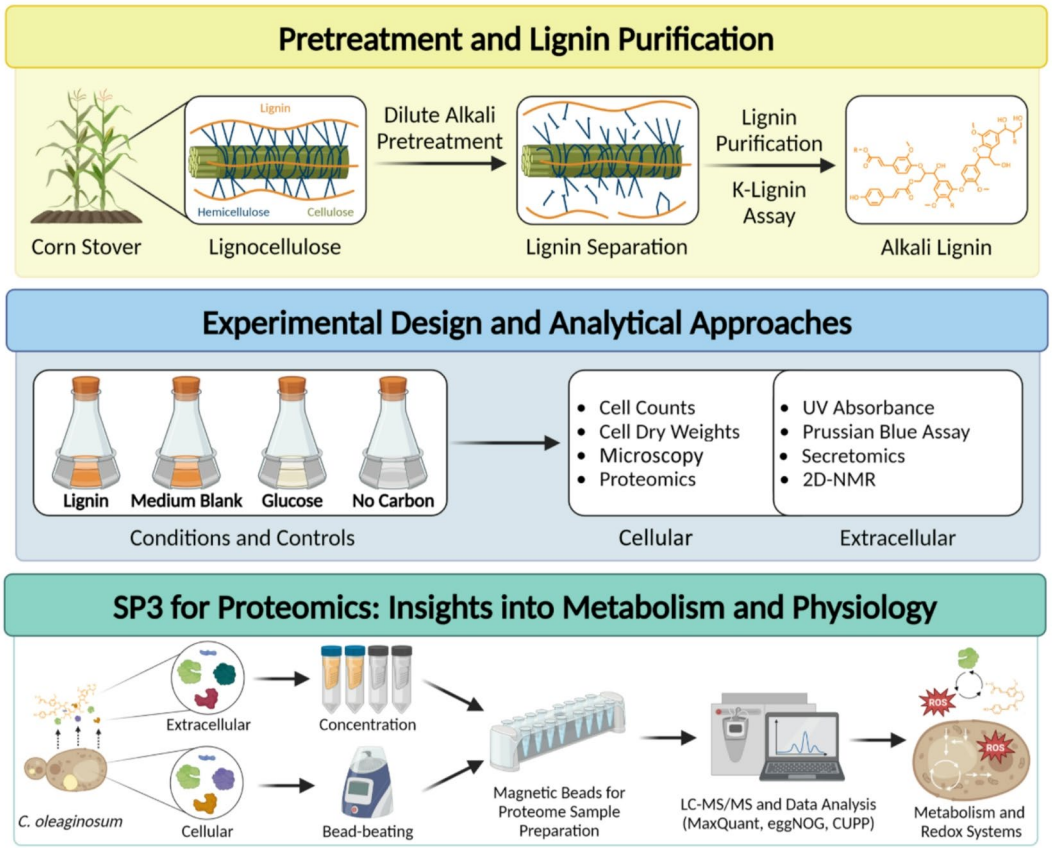

Fig. 1. Summary of the approach used in this study. First, alkali lignin was extracted from dilute alkali pretreated corn stover black liquor. Then, *C. oleaginosum* was cultivated in a YNB-based medium containing either 1 g/L of the extracted lignin, glucose, benzoate, or no additional carbon source. A medium blank containing 1 g/L lignin was also included in the appropriate analyses. A variety of assays and analytical tools were used to collect extracellular and (intra)cellular metrics for growth, lipid content, lignin modification, and lignin/aromatics transport. Finally, a label-free SP3 proteomics workflow was employed to discover putative reactive oxygen species (ROS)-mediated mechanisms and pathways for lignin modification and aromatics degradation.

titrations and analyzed via the K-Lignin assay. The overall lignin component was 87.06% with a low ash content of 0.30% (*SI Appendix*, Table S1). Though the isolated lignin contained structural saccharides, the high lignin and low ash contents are ideal for this work. Four conditions were evaluated in this study: 1 g/L lignin, 1 g/L glucose, 1 g/L benzoate, and a "No Carbon" control in which no additional carbon source was added to the base medium. The "No Carbon" control was included to uncover differences specifically attributed to interactions with lignin. An additional control of uninoculated medium with 1 g/L lignin ("medium blank") was included to check for contamination and as a baseline comparison for absorbance assays. Additional analyzes of growth, lignin modification, and lignin uptake were conducted to lay a foundation for studying the extracellular and cellular proteomes of *C. oleaginosum*.

After 144 h of cultivation, a decrease in cell dry weight (CDW) was observed for the lignin condition (Fig. 2A). Despite this, 8.5% and 11.3% decreases in lignin content were observed at 96 and 144 h, respectively, according to UV absorbance at 320 nm (Fig. 2B). These results were confirmed using the Prussian Blue assay (Fig. 2C). Although both assays indicated a relative decrease after 96 h, both methods have limitations: UV absorbance can be confounded by proteins and other secreted metabolites, while the Prussian blue assay primarily detects phenolics. The 96-hour time point was chosen to compare the CDWs of different carbon-limited conditions. Unexpectedly, a slight albeit significant difference between the "No Carbon" and lignin conditions was recorded and was supported by an increase in viable cell counts with minimal differences in cell viability (Fig. 2D–F). It's possible that the observed difference in growth is due to utilization of structural saccharides and/or acetyl groups, which constitute ~ 13% of the alkali lignin (*SI Appendix*, Table S1). At 96 h, lipid titers and fatty acid compositions for the "No Carbon" and lignin conditions were similar (*SI Appendix*, Fig. S1). Stearic acid (C18:0) was not observed in these two conditions, and a general increase in fatty acid desaturation was apparent. These results indicate that lipids were mobilized in the "No Carbon" and lignin conditions for carbon and energy generation[37,38]. Overall, increased growth in the lignin condition vs. the "No Carbon" condition was unexpected because of the sheer recalcitrance of lignin; however, this difference was minimal, and it's unclear if lignin contributed specifically to growth.

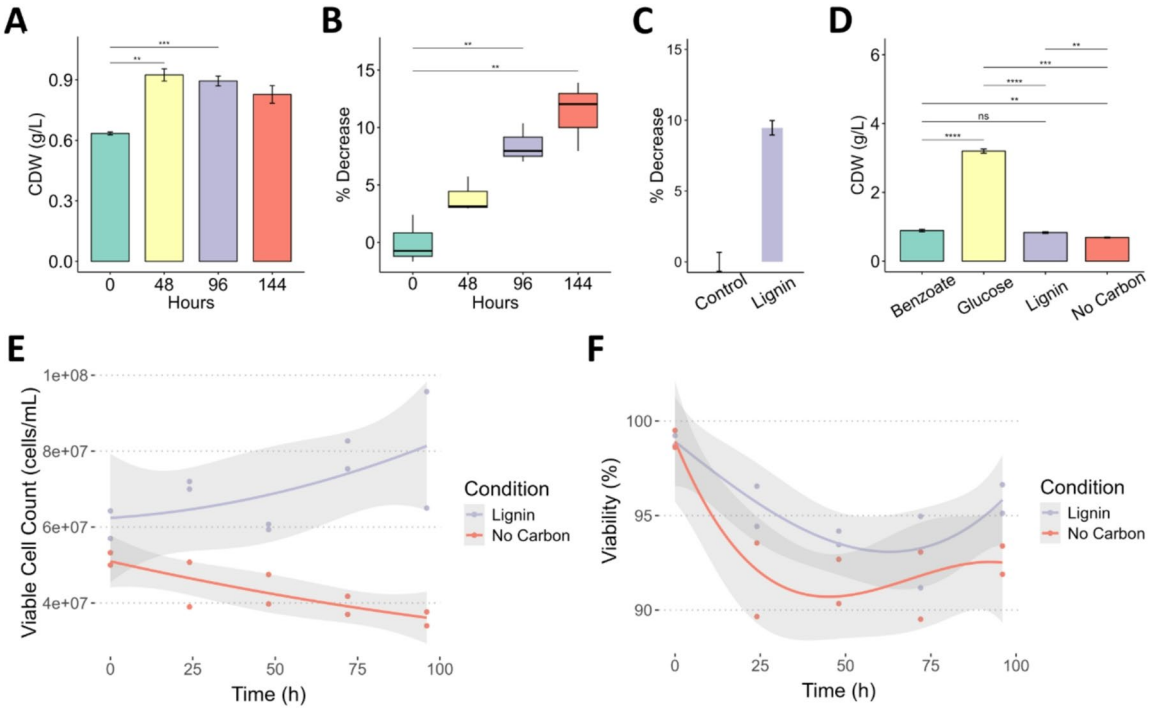

Fig. 2. *C. oleaginosum* can degrade lignin but cannot efficiently utilize it for growth. (**A**) Bar chart of cell dry weights (CDW) from cultivation on alkali-purified lignin. (**B**) Box plot showing the % decrease in UV absorbance (320 nm) of culture supernatants from the lignin condition compared to an unincubated ("0 hour") medium blank containing 1 g/L lignin. The 0 h time point designates the absorbance median and range (variation) for the medium blank. (**C**) Bar chart presenting the % decrease in absorbance at 96 h according to the Prussian blue assay. (**D**) CDWs after 96 h of cultivation on other carbon sources. (**E**) Line plot of viable cell counts over time for the lignin and "No Carbon" conditions. (**F**) Line plot of % cell viability over time according to trypan blue staining. Colored regression lines are included with gray shading that delineates 95% confidence intervals. Results shown in panels A–D are derived from biological triplicates, and the error bars represent one standard deviation. Significance levels from two-sample *t*-tests are included as asterisks in the bar charts and box plots (* = p-value < 0.05, ** = p-value < 0.005, and so on). Not significant = "ns".

NMR results demonstrate selective modification of alkali lignin

Two-dimensional (2D) heteronuclear single-quantum correlation (HSQC) NMR spectroscopy was used to study the effects of *C. oleaginosum* on lignin's chemical structures (Fig. 3A–B). HSQC provides a semi-quantitative analysis of lignin's structural features such as monolignol composition and interunit linkages. Lignin recovered from the lyophilized yeast culture supernatant was compared to the control alkali lignin (medium blank). NMR analysis revealed changes to lignin structures after yeast cultivation (*SI Appendix*, Table S2). The control lignin had a S/G/H ratio of 57:31:12, whereas after yeast fermentation, the lignin in the supernatant had a ratio of 66:29:5. Compared to the control, this is approximately a 57% decrease in the H-lignin unit, which is comprised of the *p*-coumaryl alcohol monomer. This suggests that the yeast preferentially attacks un-methylated H-type lignin

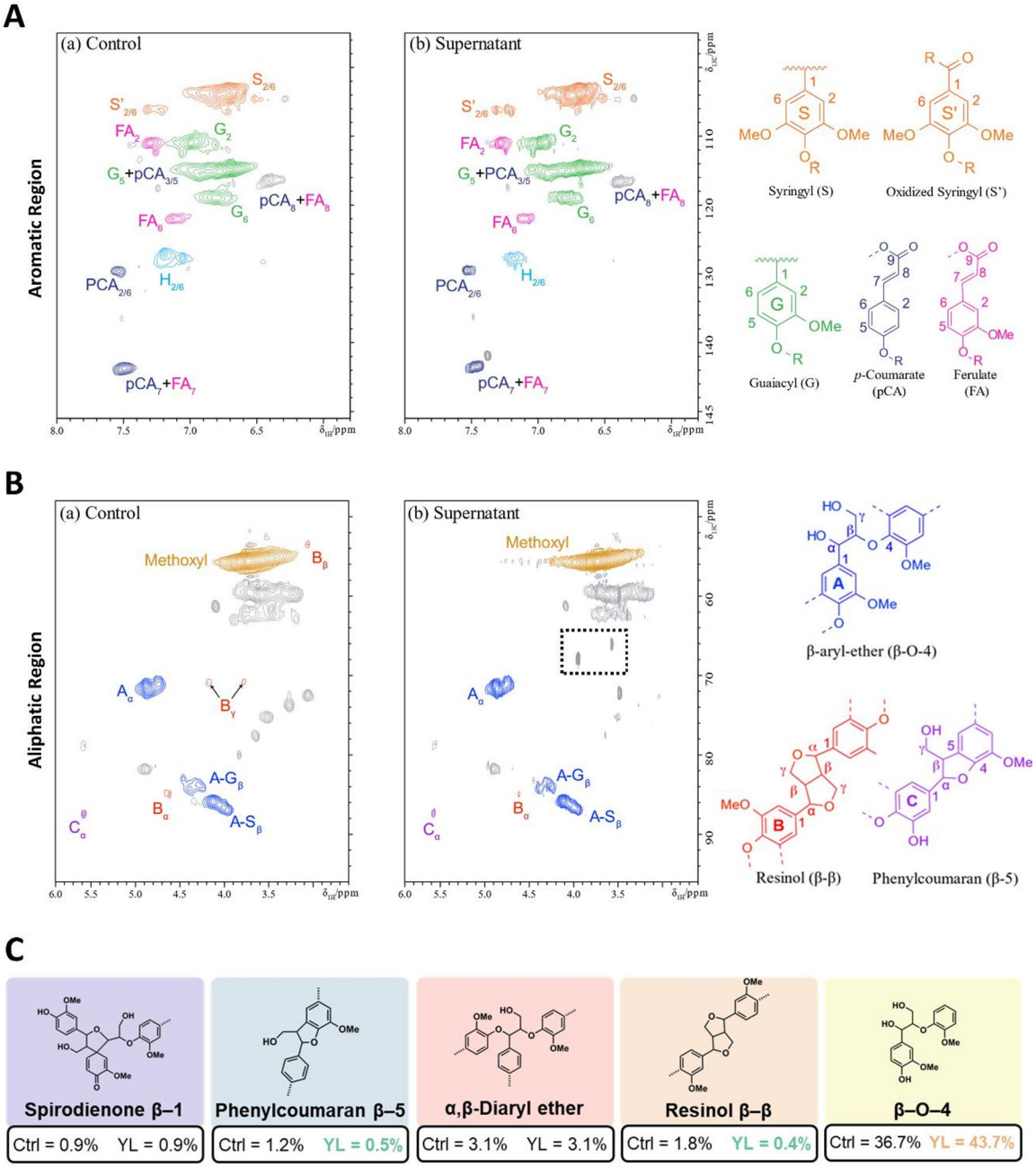

Fig. 3. NMR results pinpoint lignin structural modifications due to yeast cultivation. (**A**) Aromatics region of 2D-HSQC-NMR spectra for control lignin and lyophilized supernatant collected after 96 h of yeast cultivation with lignin. Abbreviations and the corresponding features are defined below the spectra. (**B**) Aliphatic region of 2D-HSQC-NMR spectra. Note that the five grey dots adjacent to Bγ designate xylan. Dashed black box inlay designates newly formed peaks likely due to cleavage of bonds between lignin subunits. (**C**) Summary of semi-quantitative changes to interunit lignin bonds. Note that the increase in β-O-4 can be explained by repolymerization or a relative decrease in other bonds as well as lignin motifs shown in panels **A** and **B**.

substructures, or that *p*-coumarate, *p*-hydroxybenzoate, and *p*-hydroxyphenol pendents are more susceptible to liberation. Predominant release of these H-lignin derived aromatics was reported recently and lends some support to the latter[39]. It follows that we observed a 16.5% decrease in *p*-coumarate esters and a 13.4% decrease is ferulate esters as previously reported[25]. We did not observe a significant decrease in the S/G (syringyl/guaiacyl) ratio, whereas a minor potentially insignificant decrease was observed previously using alkali-pretreated corn stover[25]. It is possible that a simulatenous decrease in S/G motifs occurred or these substructures are simply not modified.

The aliphatic region showed a 75.8% and 60.5% depletion of resinol (β-β) and phenylcoumaran β-5 linkages, respectively (Fig. 3B–C). Interestingly, there was a slight increase of the overall β-O-4 linkage signal. Among the various types of β-O-4 linkages, a small decrease in G/H-type was observed, but the S-type β-O-4 linkage dominated. The decrease of G/H-type β-O-4 could be attributed in part to the decrease of H-type β-O-4 linkage, consistent with the decrease of H-unit as observed from aromatic regions of the HSQC spectra. Previous 2D-NMR results of this yeast grown on alkali-pretreated corn stover demonstrated no decrease in β-O-4; however, the high presence of contaminating polysaccharides complicates interpretation[25]. The two new cross peaks at δ_C/δ_H 68.2/3.91 and δ_C/δ_H 72.2/3.48 ppm in the aliphatic region correspond to Ar-CH(OH)-O-CH_2-COOH. In studies of another basidiomycete yeast as well as a white rot fungus cultivated on lignin, 1D-NMR results demonstrated that these newly formed peaks may arise from the cleavage of bonds between lignin subunits or from oxidation/reduction reactions, formation of new functional groups, condensation, or repolymerization[13,40]. Compared to those and other studies, a 96-hour time point caused apparent changes in lignin structures, but longer cultivation time may be needed to observe lignin degradation[11,12,14,41]. However, a decrease in ligninolytic activity during prolonged cultivation has been reported[42], and our results, nevertheless, directly demonstrate the lignin-modifying capacity of *C. oleaginosum*.

Secretomics and proteomics reveal stark contrasts between carbon-limited conditions

Teasing out differences in protein expression due to the presence of lignin is crucial for discovering ligninolytic oxidoreductases and related enzymes. The single-pot, solid-phase-enhanced sample preparation (SP3) approach facilitated lignin removal from culture supernatants yielding high protein recoveries and digestion efficiencies (< 10% missed cleavage) as well as a higher proteome coverage per sample (> 43% total coverage of the modeled genome) compared to recent studies of *C. oleaginosum* (*SI Appendix*, Supporting Text and Tables S3–5)[43,44]. In the secretomics results, 245 unique proteins passed the SignalP signal peptide prediction score of 0.85, and 14 of these were only observed in the lignin condition (Fig. 5A and *4SI Appendix*, Dataset S1)[45]. 3,579 unique proteins were observed in the proteomics results with 56 of those only observed in the lignin condition (Fig. 4A and *SI Appendix*, Dataset S2). The Pearson correlation coefficients for lignin vs. glucose replicates were ~ 0.60 and ~ 0.90 for the secretomics and proteomics results, respectively (Fig. 4B–C). Proteins unique to the lignin condition were also observed for the lignin vs. "No Carbon", along with a lower Pearson correlation coefficient (~ 0.80) for the secretomics data (*SI Appendix*, Fig. S2A–B). For cellular proteomics results, correlation between lignin vs. "No Carbon" samples was high (~ 0.97), which is expected due to carbon starvation (*SI Appendix*, Fig. S2C). Nevertheless, principle component analyses show a clear separation for each condition (*SI Appendix*, Fig. S3).

Carbohydrate active enzyme (CAZymes) and differential expression results are summarized in Fig. 4D–E. CAZy annotations from the Conserved Unique Peptide Patterns (CUPP) platform were used because of the protein-grouping capabilities of the CUPP algorithm, which can help distinguish certain functional annotations beyond CAZy subfamilies[46]. 42 CAZymes were observed in the secretome, while 51 were observed intracellularly (Fig. 4D). For both the secretomics and cellular proteomics datasets, relative quantification was performed using LFQ intensities ("DE-filtered", Fig. 4D). In the lignin vs. glucose secretomics data, 45 proteins had $\log_2$ fold changes ("FC") > 1 and adjusted *p*-values < 0.05, while 44 were significantly downregulated (Fig. 4E). In the cellular proteomics data, 207 proteins were upregulated, and 130 were downregulated. To provide an overview of these results, pathway enrichment was conducted (Fig. 4F). It's evident that an expression regime was upregulated to access diverse carbon sources (e.g., galactose, sucrose, flavonoids/aromatics, glycans, etc.) during carbon limitation. Upregulation of N-glycan synthesis suggests restructuring of the cell wall perhaps in response to stress. Lastly, the prevalence of amino acid and other carbon recycling pathways (e.g., fatty acid degradation) was expected; however, it is intriguing to see downregulation of glutathione and cysteine/methionine metabolic pathways. This may highlight the importance of antioxidants during carbon limitation[47] and raises questions about the toxicity of lignin/aromatics and byproducts of lignin breakdown. With comprehensively analyzed proteomics results, we projected an extracellular mechanism for yeast lignin modification (SI Appendix, Fig. S4) and routes for funneling aromatics to central metabolism (Fig.). These exploratory results are detailed in the following subsections.

C. oleaginosum may express oxidoreductases for extracellular quinone redox cycling

Lignin degradation is an oxidative extracellular process involving the concerted effort of reactive oxygen species (ROS), Fenton chemistry, and various enzymes[48–50]. This complex process requires extracellular production of ROS and aromatic radicals including hydrogen peroxide (H_2O_2), hydroxyl radical ($^{-\bullet}OH$), superoxide ($O_2^{-\bullet}$), cation radicals, and phenoxy radicals[48,49,51]. These highly reactive species can be harnessed by electron-transferring auxiliary activity (AA) family oxidoreductases to attack lignocellulose[52]. In addition to a repertoire of laccases (AA1) and peroxidases (AA2), fungi also employ non-enzymatic mechanisms to modify lignin[53–57]. At the heart of this mechanism is the hydroquinone-quinone redox cycle that reduces Fe^{3+} to ultimately produce H_2O_2 for initiating enzymatic catalysis, and $^{-\bullet}OH$ to react directly with lignin units[51,58]. Interestingly, whether or not basidiomycete yeasts have the functional capacity for quinone redox cycling has yet to be addressed according to a thorough literature review and the following wildcard search queries using Web of Science and

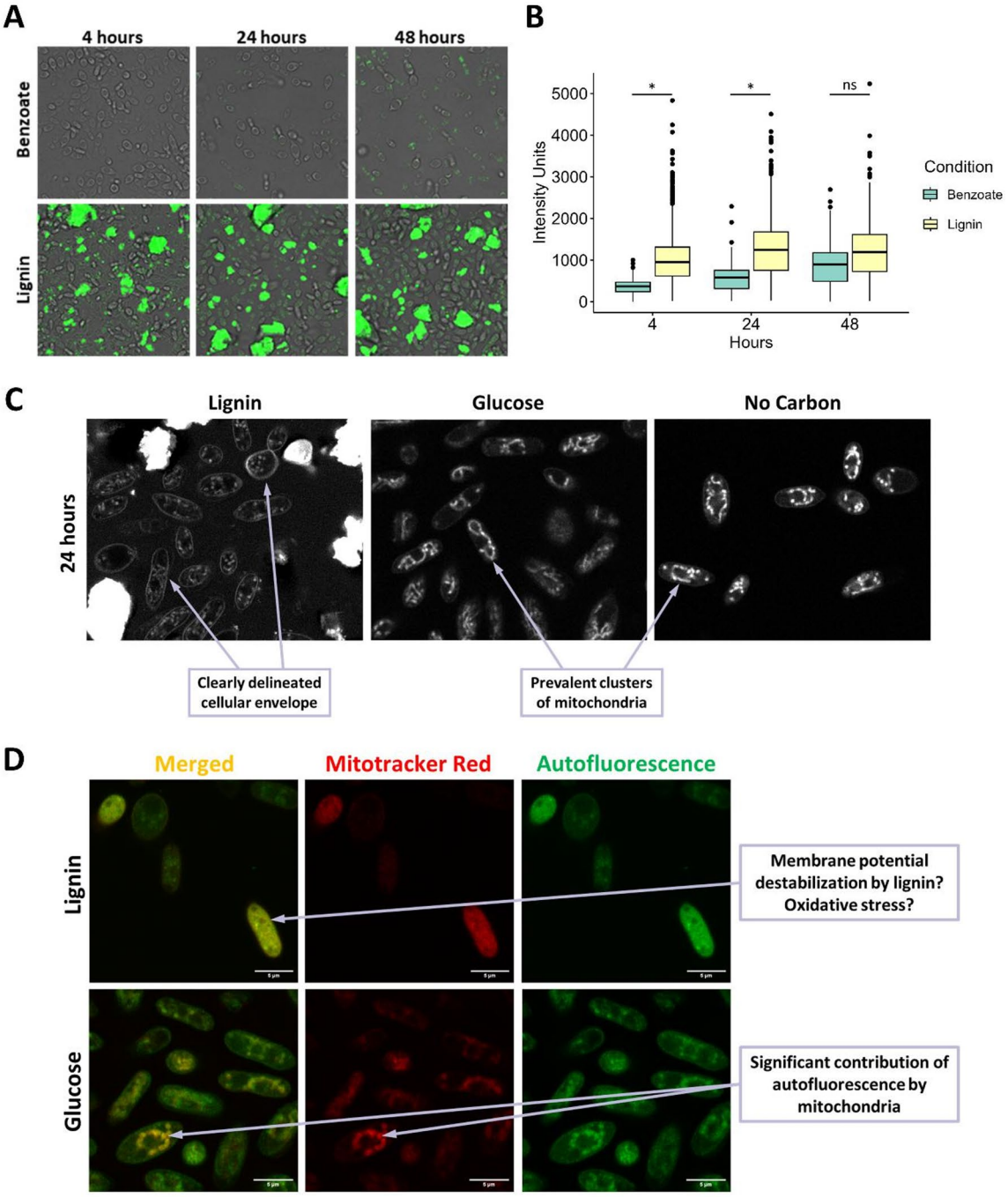

Fig. 4. High-resolution microscopy reveals lignin-dependent yeast cell fluorescence and morphological differences. (A) Fluorescence microscopy results showing lignin autofluorescence and subtle differences between lignin and benzoate cultures. (B) Fluorescence intensity distributions for cell populations recorded over time. (C) Airyscan images show difference in fluorescence of the cellular envelope and putative mitochondrial clusters. (D) Airyscan images of yeast labeled with MitoTracker Red CMXRos Dye. 5 µm scale bars are shown in the bottom right corners for Panel D. Differences in yeast fluorescence intensities may be attributed to mitochondrial autofluorescence, lignin interactions, and/or carbon-limited oxidative stress[47]. For panel B, cell population fluorescence intensities for three images were averaged then these three mean values were used for t-tests. Significance levels from two-sample t-tests are included as asterisks in the box plots. One asterisk is a p-value of 0.05. No significant difference is "ns"

PubMed: ((yeast) AND (hydroquinone redox cycl* OR quinone redox cycl* OR Fenton chemistry)) AND (lignin OR aromatic*).

There are several requirements for the hydroquinone redox cycle: oxidoreductases, reductants, and an acidic pH[51,59]. A combination of BLASTp searches and CAZy CUPP annotations were used to find candidates

in our proteomics data (*SI Appendix*, Fig. S4 and Dataset S3)[46,52,60]. Ferric reductases are important for iron uptake (generally as Fe^{2+}) and maintaining an active quinone redox cycle[61,62]. Unfortunately, none of the ferric reductases annotated in the Joint Genome Institute (JGI) database were observed intracellularly; however, they were observed in the secretome (*SI Appendix*, Dataset S4), despite likely being localized to the cell membrane[61,63]. These include Co_368607 and Co_366398 (the latter only observed in lignin replicates), which share 35–40% identity but only 20–35% coverage with a ferric reductase (Pospl1_130030) from the model brown rot fungus *Rhodonia placenta* MAD 698R (*SI Appendix*, Dataset S3)[64,65]. Co_414234 was also only observed in the lignin condition and has a ferric reductase transmembrane component-like domain (IPR013130)[66], even though it was not observed in the BLASTp searches. In the absence of ferric reductases, Fe^{3+} can still evolve as a result of Fe^{2+} oxidation and participate in oxidation of hydroquinone and semiquinone species[58]. Fe^{2+} can react with oxygen to generate $O_2^{-\bullet}$ and with H_2O_2 to produce $^{-\bullet}OH + {}^{-}OH$—the latter may partially explain the observed pH increase in the lignin-containing cultures (*SI Appendix*, Fig. S4).

H_2O_2 can be generated from other sources including $O_2^{-\bullet}$[51]. Superoxide dismutase (SOD) catalyzes the conversion of $O_2^{-\bullet}$ to H_2O_2 and is an essential antioxidant for combatting oxidative stress[51]. Though localization predictions from other *Tremellomycetes* loosely related to *C. oleaginosum* suggest intracellular localization, there are several fungi that secrete SOD variants[51,67]. Two copper/zinc-dependent SODs (Co_394365 and Co_419771) with predicted signal peptides and secretion predictions were observed[68]. Co_419771 was significantly upregulated in the lignin condition (FC 6.51), which suggests severe oxidative stress (*SI Appendix*, Dataset S4). Glucose–methanol–choline (GMC) oxidoreductases (AA3), glyoxal oxidases (AA5_1), and oxalate oxidases can also produce H_2O_2 using a variety of reductants[52]. GMC oxidoreductases (AA3_2) can utilize aryl-alcohols and sugars as electron donors, whereas glyoxal oxidases convert simple aldehydes to carboxylic acids[69,70]. Oxalate is an important iron chelator during wood decay, and is detoxified to carbon dioxide and H_2O_2 via oxalate oxidase[71,72]. Two GMC oxidoreductases were observed extracellularly (Co_352536 and Co_372521) and one intracellularly (Co_342568; DEP FC 4.93). The first two GMC oxidoreductases belong to CUPP branch AA3:6.5, while the other may have a different function as it is categorized in CUPP branch AA3:10.1 (*SI Appendix*, Dataset S4). Two glyoxal oxidases were observed in the secretomics dataset (Co_344356 and Co_26860). The latter had a signal peptide prediction score of 0.69 but was significantly upregulated in the lignin condition (FC 2.26). An enzyme of the cupin superfamily (Co_373698) was also significantly upregulated (FC 2.73) and is classified as an oxalate oxidase (or superoxide dismutase) by InterPro (IPR001929)[66]. Two putative sulfate/bicarbonate/oxalate exchangers were observed in the proteomics results: Co_335524 and Co_352469, which was only observed in the lignin condition.

Laccases and quinone oxidoreductases play significant roles in quinone redox cycles. Laccases are multicopper oxidases that use O_2 to oxidize hydroquinones to semiquinones[53,73]. Semiquinones are unstable products that undergo autooxidation to form quinones[58]. Two putative laccases with predicted signal peptides were upregulated in the secretome of the lignin condition: Co_368910 (FC 5.57) and Co_369862 (FC 5.68) (Step 1 in Fig. 6 and *SI Appendix*, Fig. S4). Unlike the former, Co_369862 shares some homology with laccases from the white-rot fungus *Trametes versicolor* (> 30% identity and > 30% coverage; *SI Appendix*, Dataset S3). Another putative laccase Co_416150 shares > 37% identity but only ~ 25% coverage with a laccase from *T. versicolor* (*SI Appendix*, Dataset S3). Co_416150 was observed but downregulated in the secretome (FC -0.96)[74]. Interestingly, this enzyme was only observed in the cellular proteome of the lignin condition. Although they share low sequence coverage (20–35%) against *T. versicolor* laccases, Co_368910, Co_372508, and Co_416150 are secreted AA1 CAZymes according to MULocDeep prediction, and the first two are members of CUPP branch AA1:73.1[68]. In contrast, Co_369862 may locate to the cell membrane and was downregulated (FC -3.29)[68]. It is a member of the subfamily AA1_2, which includes ferroxidases that oxidize Fe^{2+} to modulate Fenton reactions and decrease $^{-\bullet}OH$[75,76]. Indeed, the eggNOG annotation for this enzyme was FET3, a ferroxidase involved in iron uptake. Studies of FET3-like proteins in basidiomycetes show that these multicopper oxidases ostensibly have dual ferroxidase/laccase activities[74,77–79]. Nonetheless, this enzyme shares 30–45% identity and 30–35% coverage with phenol-oxidizing laccases from *T. versicolor* (*SI Appendix*, Dataset S3)[74,77,80]. It is likely that the laccase candidates discussed herein require phenolic mediators for oxidation and have lower redox potentials than those of white rot fungi. Nevertheless, more research into putative yeast laccases is clearly needed.

Quinone oxidoreductases including 1,4-benzoquinone reductase (AA6) are involved in aromatics degradation and protection against reactive quinones[52,81–83]. A putative quinone oxidoreductase (Co_369953; FC 0.69) and two annotated 1,4-benzoquinone reductases (Co_380727, FC 1.30; Co_164578, FC 0.66) were upregulated to various extents in the lignin condition of the proteomics results (*SI Appendix*, Fig. S4). According to BLASTp results, these enzymes share > 45% identity and > 65% coverage with quinone oxidoreductases from *Rhodonia placenta* (*SI Appendix*, Dataset S3)[65]. Moreover, Co_380727 is a predicted cell membrane protein, which has > 45% identity and > 65–70% coverage with functionally characterized quinone oxidoreductases from the white rot fungus *Phanerochaete chrysosporium* and brown rot fungus *Gloeophyllum trabeum*[68,82,84]. A cyptoplasmic protein Co_342726 only observed in the lignin replicates was annotated as QOR1, a quinone oxidoreductase, by eggNOG; nevertheless, a conserved domain search on NCBI returned a prostaglandin dehydrogenase (cd05288), which is a surprising annotation for yeast and complicates its interpretation[85].

In addition to the quinone redox cycle, peroxidase-catalyzed oxidation of lignin also generates benzoquinones, among other degradation intermediates[81,86]. Though many peroxidases were observed in the secretome (Co_396749, Co_237718, Co_382630, and Co_372514), none of them were upregulated, and only one (Co_396749) had a secretion prediction (Step 2 in Fig. 6 and *SI Appendix*, Dataset S4)[68]. Given that both the glucose and lignin culture conditions were carbon-limited, this may be explained by general upregulation of genes under carbon catabolite derepression[87]. Peroxidase expression may also be a function of culture conditions like nitrogen source as Martinez et al. observed with *Pleurotus eryngii*[58,88]. Nevertheless, peroxidase activity has been observed with *C. oleaginosum* and another *Trichosporonaceae* yeast[14,89]. BLASTp results of

Fig. 5. Distinct protein expression patterns in lignin and glucose conditions uncovered by secretomics and proteomics. (A) Venn diagrams indicating overlap of unique, quantifiable protein IDs. Only one missing LFQ intensity value was permitted among the replicates of each condition. Secretomics results were filtered using a cutoff of 0.85 according to SignalP 6.0[45]. (B) Correlogram of Pearson correlations for overlapping LFQ results from secretomics data. (C) Correlogram of Pearson correlations for proteomics data. (D) Donut charts of CUPP-annotated CAZymes found in our secretomics and proteomics data[46]. "Observed" refers to all unique identifications. "DE-filtered" refers to IDs for which two LFQ values were present to conduct differential expression analysis. (E) Volcano plots summarizing FCs from separate differential expression analyses of secretomics and proteomics data. The vertical purple lines designate FCs of −1 and +1, whereas the dashed black line designates an adjusted p-value of 0.05. (F) Summarized dot plot results from KEGG pathway enrichment analysis[198, 199] using protein IDs with significant differences (adjusted p-value ≤ 0.05) in expression: "Down" refers to those with FC ≤ −1, and "Up" refers to FC ≥ 1.

AA2 peroxidases from *T. versicolor*, *P. chrysosporium*, and the recently isolated relative *Cutaneotrichosporon cavernicola* yield Co_382630 and Co_372514 with > 55% coverage and identity (*SI Appendix*, Dataset S3)[51,90]. Interestingly, these enzymes were not annotated by CUPP nor were AA2 CAZy annotations included for these entries on JGI[46,52,91,92]. Based on the aforementioned and because these enzymes do not have predicted signal peptides, it's likely that these enzymes are AA2 class I peroxidases. This class of peroxidases has lower redox potentials than class II lignin and manganese peroxidases, and they are generally involved in oxidative stress response[93].

Theoretically, these proteomics results suggest a capacity for quinone redox cycling by *C. oleaginosum*, even though the reactivity of Fenton chemistry would be suboptimal under the near neutral culture conditions studied here (starting pH of 6.5; see *SI Appendix*, Fig. S4)[59]. To bolster this conclusion, the mechanisms by which hydroquinones are generated *de novo* and secreted to help initiate redox cycling will need to be studied in yeast. Hydroquinone secretion has been observed with filamentous fungi; however, it is unclear what transporters are involved because few have been functionally characterized[55,94,95]. Of course, this is also the case for the other candidate enzymes discussed hitherto—direct functional genomics analyses will be essential for resolving ambiguities regarding this yeast's laccase and peroxidase activities[14,25]. Overall, these findings highlight the need for additional research to validate the proposed candidates and probe the quinone redox cycling potential of *C. oleaginosum* and other yeasts.

C. oleaginosum may uptake poymeric lignin but the mechanism remains unclear

Transport mechanisms for lignin-derived aromatics in yeast are underexplored[96,97]. In bacteria and filamentous fungi, active transport of monoaromatics involves ATP-binding cassette (ABC) transporters and major facilitator superfamily (MFS) transporters[33]. Passive transport has also been suggested, though most research has been conducted in bacteria which have drastically different cellular envelopes[30,98]. Proteomics can help elucidate potential aromatics transporters by highlighting those that are upregulated or only observed in a particular condition. We observed 380 of the 790 JGI-annotated transporters[91,99]. The relative abundances of 246 were quantified for lignin vs. glucose: 48 were upregulated (FC > 0.8) while 18 were downregulated (FC < − 0.8). Two enzymes annotated as *p*-coumarate-CoA synthases were upregulated (Co_383485, FC 2.57; and Co_386597, FC 1.26; *SI Appendix*, Dataset S2). These are annotated members of a Fatty Acid Group Translocation Family that use ATP to attach CoA to *p*-coumarate and other aromatics in a process that may be coupled to transport[68,91,99]. Upregulation of these enzymes is in line with a decrease in H-lignin (Fig. 3A and C). Enzymes with cell membrane localization predictions include an arabinose, xylose, and/or aromatics transporter (Co_378211; FC 0.83), a MFS transporter (Co_419501; DEP FC 3.06), and an amino acid transporter (Co_391320; FC 1.37) with a phenol hydroxylase domain (IPR012941) (*SI Appendix*, Dataset S4)[66]. A MFS high affinity nicotinate permease (Co_96030) and an ABC transporter (Co_345222) were observed exclusively in the lignin condition. The latter is annotated as a plant cuticular wax and/or lipid exporter. Plant cuticles have complex compositions that include aromatics[100]. Lastly, a MFS quinate: H + symporter (Co_96856) was only observed in the lignin condition. Fewer transporters were upregulated in our results compared to a recent study of the yeast *Rhodosporidium fluviale* cultivated on black liquor, but this may be due to substantially higher aromatics concentrations in their medium[28]. We also conducted searches using hydroxybenzoate transporters recently characterized in the pathogenic yeast *Candida parapsilosis*, but no high-scoring alignments were found (*SI Appendix*, Dataset S3)[101].

A recent publication reported active transport and subsequent degradation of an aromatic dimer by *P. chrysosporium*[97]. However, there is limited research explicitly addressing lignin polymer uptake in microbial systems. We speculate that polymeric lignin can be internalized by *C. oleaginosum* based on research involving uptake of polyaromatic polystyrene in yeast[34,102,103]. As a preliminary investigation, we used confocal fluorescence microscopy to harness the autofluorescent signatures of lignin and study its uptake (Fig. 5A–B and results from medium blank in *SI Appendix*, Fig. S5)[35,36]. We employed the cell segmentation software Cellpose to analyze yeast autofluorescence using various controls[104–106]. Cellpose identified cells with high accuracy even in the presence of lignin particles (*SI Appendix*, Fig. S6A). Thereafter, fluorescence intensities of identified cells were recorded. Though unapparent to the naked eye, cells in the lignin condition have significantly higher fluorescence intensities for all comparisons except lignin vs. benzoate at 48 h (Fig. 5B and *SI Appendix*, Fig. S6B–C). It's possible that the increase in yeast autofluorescence confounds any differences, perhaps due to carbon-limited stress response and/or aromatics toxicity, given that 1 g/L benzoate is close to the minimum inhibitory concentration of *C. oleaginosum*[22,104,107,108]. We also performed super resolution fluorescence imaging to illustrate structural changes due to lignin interactions (Fig. 5C). For cells without lignin, the weak autofluorescence is consistent with the structure of mitochondria. With lignin the fluorescence is more punctate and widespread throughout the cell, indicating significant changes to subcellular morphology. Moreover, there is a clear delineation of the cellular envelope in the lignin condition, which may represent lignin association/adsorption to the cellular wall/membrane. Nevertheless, the spatially-resolved fluorescence microscopy images show that fluorescence inside cells is stronger in the lignin condition. Using a dye to label mitochondria, the observed autofluorescence in the absence of lignin is partially due to mitochondria, whereas in the presence of lignin there is no apparent dye localization (Fig. 5D). This suggests drastic changes to subcellular processes and possibility of lignin-induced membrane destabilization, which has been observed using other nanoparticles (*SI Appendix*, Supporting Text)[109]. Overall, these results suggest the possibility of polymeric lignin uptake by *C. oleaginosum*, but investigations employing labeled lignin nanoparticles and electron microscopy will be needed to validate and explore mechanisms.

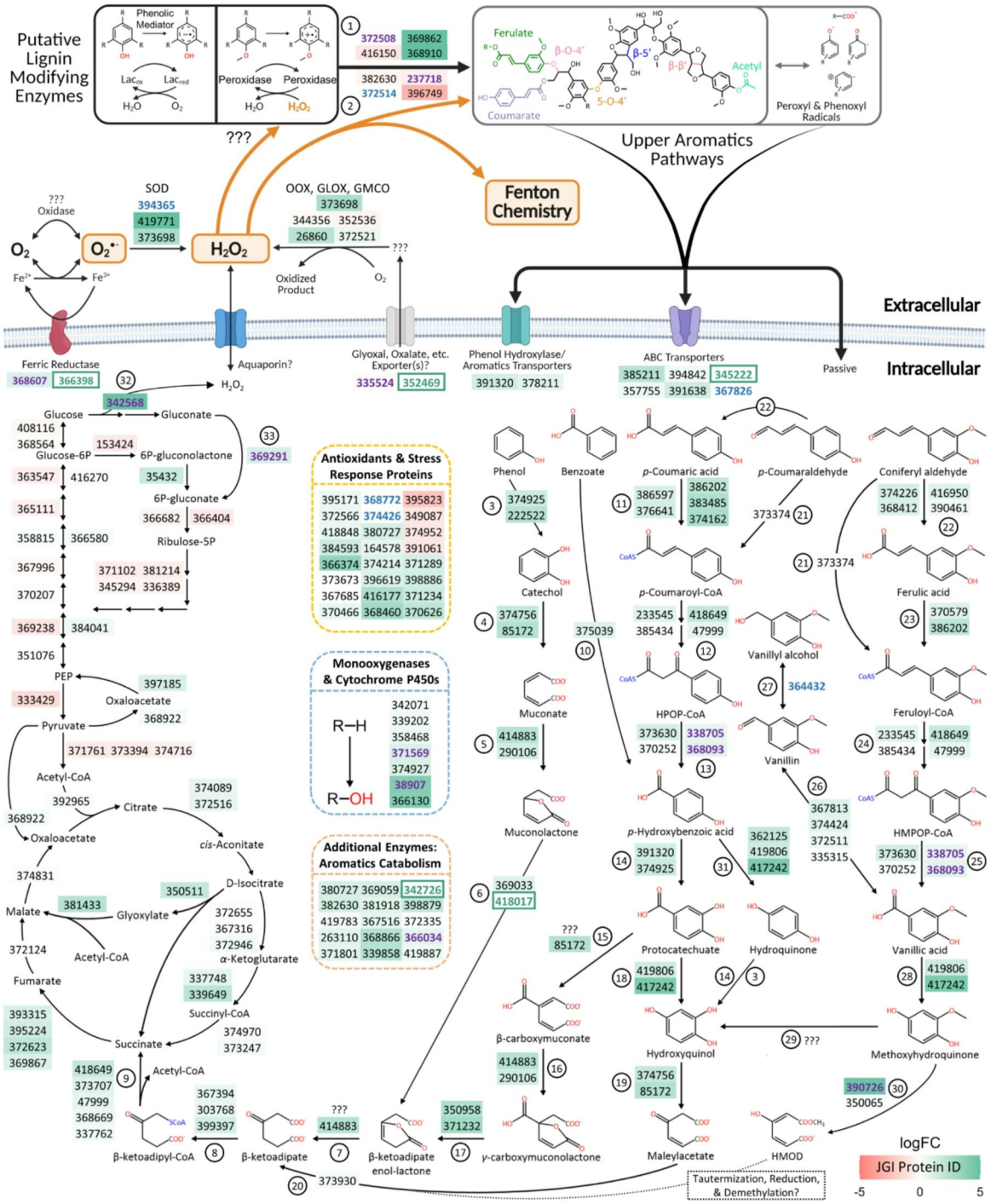

Pathways for aromatics catabolism are upregulated in the lignin condition

Yeasts funnel aromatic monomers to intermediates such as protocatechuate, catechol, and hydroxyquinol via intricate upper pathways[110]. Dioxygenases cleave the aromatic rings yielding intermediates that are metabolized through lower pathways (e.g., branches of the β-ketoadipate pathway), ultimately leading to central metabolites[111,112]. Aromatic catabolic enzymes and the corresponding pathways are largely uncharacterized in *C. oleaginosum*. In an earlier report, cleavage positions for catechol, protocatechuate, and hydroxyquinol were assayed using clarified lysates[25]. Catechol and hydroxyquinol underwent *ortho*-cleavage, whereas cleavage of proteocatechuate was negligible suggesting that it is decarboxylated to hydroxyquinol or catabolized via some other route. They also functionally annotated a catechol dioxygenase (homolog of Co_374756) that has intradiol and extradiol ring-cleaving activities. Beyond these analyses, specific catabolic pathways were not proposed; therefore, we scoured publications in which aromatics catabolic enzymes were functionally characterized in fungi (and some cases bacteria). We then conducted extensive BLASTp searches against proteins observed in our proteomics results to project putative aromatics catabolic pathways in *C. oleaginosum* (*SI Appendix*, Datasets S1–3)[60]. Rationalized by our 2D-NMR results and by the significance of ferulate G-lignin monomers in corn

◀**Fig. 6**. Proposed pathways for lignin modification and catabolism of lignin-derived aromatics. According to our NMR results, extensive homology searches, and literature review, pathways are only shown for H- and G-lignin-derived aromatics. Additional details regarding ROS-mediated mechanisms for lignin modification are provided in the SI Appendix, Fig. S4. The predicted pathways for G-lignin derivatives are discussed in SI Appendix, Supporting Text. JGI protein IDs are included within boxes that are colored according to the average FC for lignin vs. glucose. Note that boldface green lettering corresponds to proteins only observed in the lignin condition. Boldface blue lettering corresponds to proteins that were observed, but for which no differential expression analysis could be conducted due to missing intensity values. Boldface purple lettering corresponds to IDs for which raw intensity values were used in DEP differential expression analysis due to missing LFQ intensity values. Question marks and dotted arrows represent uncertain annotations. The numbers in circles designate the following putative enzyme annotations: 1. Laccases, 2. Peroxidases, 3. Phenol 2-monooxygenase, 4. Catechol 1,2-dioxygenase, 5. Muconate cycloisomerase, 6. Muconolactone isomerase, 7. β-ketoadipate enol-lactone hydrolase, 8. β-ketoadipate-succinyl-CoA transferase, 9. β-ketoadipyl-CoA thiolase, 10. Benzoate 4-monooxygenase (Cytochrome P450), 11. p-Coumarate-CoA ligase, 12. Cinnamoyl-CoA hydratase/dehydrogenase (first arrow = IDs on the left) and 3-ketoacyl CoA thiolase (second arrow = IDs on the right), 13. Thioesterase, 14. Hydroxylase, 15. Protocatechuate 3,4-dioxygenase, 16. β-carboxymuconate lactonizing enzyme, 17. γ-carboxymuconolactone decarboxylase, 18. Monooxygenase/decarboxylase, 19. Hydroxyquinol 1,2-dioxygenase, 20. Maleylacetate reductase, 21. Cinnamoyl-CoA reductase, 22. Aldehyde dehydrogenase/cytochrome P450 (see IDs below coniferyl aldehyde structure), 23. Feruloyl-CoA synthetase, 24. Cinnamoyl-CoA hydratase/dehydrogenase (first arrow = IDs on the left) and 3-ketoacyl CoA thiolase (second arrow = IDs on the right), 25. Thioesterase, 26. Vanillin dehydrogenase, 27. Vanillyl alcohol oxidase, 28. Vanillate hydroxylase, 29. O-demethylase, 30. (Di)methoxyhydroquinone 1,2-dioxygenase, 31. p-Hydroxybenzoate decarboxylase, 32. GMC oxidoreductase, 33. Gluconate kinase.

stover[113], we focused our efforts on projecting catabolic pathways for H- and G-lignin derived aromatics (refer to *SI Appendix*, Supporting Text for information about predicted G-lignin and phenol derivative pathways).

C. oleaginosum utilizes H-lignin model aromatics *p*-coumarate and *p*-hydroxybenzoate, but pathways have yet to be completely annotated[114–116]. In filamentous fungi, conversion of *p*-coumarate to *p*-hydroxybenzoate has been extensively studied[117–120]. Lubbers et al. demonstrated that *Aspergillus niger* uses a CoA-dependent β-oxidative route akin to fatty acid degradation[121]. Briefly, *p*-coumarate is converted to *p*-coumaroyl-SCoA by a hydroxycinnamate-CoA synthase (hcsA). The product is then hydrated and dehydrogenated by a multifunctional β-oxidation hydratase/dehydrogenase (foxA) to yield 4-hydroxyphenyl-β-ketopropionic acid-SCoA (HPOP-CoA). Afterwards, *p*-Benzoyl-CoA is generated by 3-ketoacyl-CoA thiolase (katA). Finally, thioesterases remove CoA to produce *p*-hydroxybenzoate. We searched our proteomics data for homologs of characterized proteins (Steps 11–13 in Fig. 6). The BLASTp scores for *Aspergilli* hcsA were fairly low, so we also searched bacterial enzymes involved in the CoA-dependent non-oxidative pathway that has been proposed for some fungi (*SI Appendix*, Dataset S3)[121–125]. Several putative proteins were upregulated in the cytoplasm and peroxisome: Co_383485 (FC 2.57; cytoplasm), Co_386597 (FC 1.26; cytoplasm), Co_386202 (FC, 2.09; peroxisome), Co_376641 (FC 1.32; peroxisome), and Co_370579 (FC 1.05; peroxisome) (*SI Appendix*, Dataset S4). Co_386597, Co_386202, and Co_376641 were loosely homologous with bacterial feruloyl-CoA synthetases (SI Appendix, Dataset S3). Only one fungal homolog of foxA was upregulated (Co_233545; FC 0.98) and contained a C-terminal peroxisomal targeting sequence[68,126,127]. BLASTp results of bacterial hydroxycinnamoyl-CoA hydratase-lyases returned Co_381918 (FC 0.93; peroxisome). Though many katA and thioesterase homologs were observed, few had peroxisomal predictions. According to MULocDeep, Co_368669 and Co_371904 are localized in the cytoplasm; however, both have C-terminal peroxisomal targeting sequences[68,126,127]. β-oxidation of fatty acids was upregulated in the lignin condition (Fig. 5F), and by extension those proteins may be candidates for unraveling CoA-dependent *p*-coumarate catabolism in *C. oleaginosum*.

Prior to ring cleavage, *p*-hydroxybenzoate is converted to hydroxyquinol (Steps 3, 14, 18, and/or 31 in Fig. 6). Phenol hydroxylase is active on phenol derivatives and has been characterized in the close relative *Cutaneotrichosporon cutaneum*[128,129]. Two potential homologs with > 33% coverage and > 50% identity were upregulated in our results: Co_391320 (FC 1.37) and Co_374925 (FC 1.64) (*SI Appendix*, Dataset S4). Co_222522 (FC 2.31) is an additional candidate annotated as a 2-phenol monooxygenase on JGI[130], though it is likely involved in ubiquinone biosynthesis. Phenol hydroxylase from *C. cutaneum* is structurally related to fungal 4-hydroxybenzoate 3-hydroxylase, so these homologs may be involved in the conversion of *p*-hydroxybenzoate to protocatechuate (Step 14 in Fig. 6)[131]. Oxidative decarboxylation of *p*-hydroxybenzoate and protocatechuate to hydroquinone and hydroxyquinol, respectively, has been reported for the yeast *C. parapsilosis* and white-rot fungi (Steps 18 and 31 in Fig. 6)[132,133]. Co_382250 was the highest scoring hit for 4-hydroxybenzoate 1-hydroxylase (i.e., MNX1) from *C. parapsilosis* but was not observed in our proteomics results, though the putative homolog Co_419806 was observed and upregulated 1.56-fold. Co_419806 has a low alignment score with MNX1 but higher scores against basidiomycete decarboxylases[132]. This is also the case for Co_417242 which was drastically upregulated (FC 4.25) and may be a homolog of a reported *T. versicolor* decarboxylase (TV_32834) that preferentially decarboxylates protocatechuate. The putative *Gelatoporia subvermispora* homolog (GS_120062) of Co_419806 displays activity against *p*-hydroxybenzoate and protocatechuate[132].

Ring cleavage detoxifies aromatics and yields assimilable carbon sources[134]. Enzymes that catabolize hydroxyquinol and protocatechuate have been investigated using *C. parapsilosis* and *A. niger*[133,135]. Based on BLASTp results, Co_374756 is the top candidate for hydroxyquinol 1,2-dioxygenase activity (FC 1.83; Step 19 in Fig. 6 and *SI Appendix*, Dataset S4). Co_85172 is an additional candidate (FC 2.44), but it had a higher E-value

(5.50E-39) against a protocatechuate 3,4-dioxygenase (NRRL3_1405) from *A. niger*. Intradiol hydroxyquinol cleavage yields maleylacetate, which is converted to β-ketoadipate by maleylacetate reductase (Step 20 in Fig. 6). Negligable upregulation of Co_373930 (FC 0.25), a homolog of the *A. niger* candidate, was observed[136]. A homolog of another candidate from *C. parapsilosis* was observed but also not differentially expressed (Co_374156 with 41% coverage and 64% identity)[137,138]. Intradiol cleavage of protocatechuate leads to formation of β-carboxymuconate, which undergoes cyclization via muconate cycloisomerase (Steps 15 and 16 in Fig. 6)[139]. The product γ-carboxymuconolactone can be decarboxylated to β-ketoadipate enol-lactone as observed in *A. nidulans* (Step 17 in Fig. 6)[140]. A homolog of the decarboxylase studied by Martins et al.[140] was not observed in *C. oleaginosum*. Thankfully, the eggNOG description of Co_371232 (FC 2.94) was "Carboxymuconolactone decarboxylase family", and the orthologous group annotation was "Sphingomonadales", which raises interesting questions about horizontal gene transfer among soil-dwelling microorganisms[80]. Two additional candidates include Co_350958 (FC 2.52; aminocarboxymuconate-semialdehyde decarboxylase) and Co_372335. Finally, β-ketoadipate enol-lactone is converted through successive reactions of the β-ketoadipate pathway to yield succinate for entry into central metabolism, with putative enzymes showing upregulation (Steps 7–9 in Fig. 6; refer to *SI Appendix*, Supporting Text for additional details).

As a whole, we speculate that mechanisms for lignin modification are present in *C. oleaginosum* and demonstrate upregulation of predicted catabolic pathways for H-lignin and G-lignin derivatives (*SI Appendix*, Datasets S1–4 and Fig. 6). It follows that entry point enzymes for the TCA cycle and glyoxalate shunt were also upregulated, whereas glycolytic enzymes were downregulated (Fig. 6 and *SI Appendix*, Dataset S4). Antioxidants are important for mitigating excess ROS such as H_2O_2, which can be generated extracellularly and re-enter the cell via direct permeation or aquaporins[51]. We observed upregulation of several antioxidants including catalases that neutralize H_2O_2 (Co_370626, FC 2.07; Co_371234, FC 1.60). Nevertheless, many of these enzymes were only partially upregulated in the lignin vs. No Carbon comparison, which speaks to their general role in nutrient-limited stress response[47]. For specific enzymes like glutathione-dependent formaldehyde-activating enzyme (Co_398886, FC 1.42), detoxification of formaldehyde from demethylation of aromatics may rationalize these differences[141]. These findings hint at similarities in aromatics catabolism between yeasts and filamentous fungi of the Agaricomycotina subphylum, yet they also underscore gaps in our understanding and the need for additional research. The lack of metabolomics results herein presents a significant opportunity for future studies but also poses challenges. These include limitations in current techniques (e.g., challenges removing lignin to prevent instrument damage), the scarcity of certain aromatics released even by white-rot fungi, and the intricate nature of lignin degradation intermediates[132,142]. Assays that directly measure ROS generation will also further our understanding of redox mechanisms involved in aromatics detoxification and lignin degradation[143]. Redox proteomics, which assesses protein oxidation, offers an innovative approach to explore how fungi manage redox homeostasis during lignin degradation[144,145].

Conclusion

In this exploratory study, we cultivated *C. oleaginosum* on alkali lignin and, according to 2D-NMR, observed modification of the H-lignin structure, *p*-coumarate and ferulate pendents, and interunit bonding. A comprehensive proteomics analysis revealed the potential for yeast quinone redox cycling as well as putative pathways for aromatics catabolism, which were upregulated in the lignin condition. Based on these results, we conclude that this yeast and likely other basidiomycete yeasts may have lignin-modifying capabilities, thereby playing salient roles in lignocellulose degradation and aromatics detoxification in native microbial communities. Nonetheless, challenges in analyzing secretomics data, especially under stressful carbon-limited conditions that may cause cell lysis, highlight the complexity of interpreting these results. Additionally, the influence of culture conditions, sampling time points, and localization of putative ligninolytic enzymes (e.g., *Cryptococcus neoformans* expresses cell well-bound laccase) further complicates ours and others' research using this yeast[146,147]. These insights call for continued exploration and refinement of methodologies to enhance our understanding of yeast-lignin interactions. This will advance efforts to metabolically engineer yeasts to express powerful, complementary ligninolytic enzymes from white-rot fungi and optimize the conversion of lignin-derived aromatics to valuable products.

Methods

A brief summary of relevant materials and methods is presented below. Additional details are included in *SI Appendix*, Supplementary Methods.

Lignin extraction from corn Stover

The National Renewable Energy Laboratory provided the black liquor fraction of dilute alkali-pretreated corn stover, which was used for lignin extraction[148,149]. The extraction process involved serial acid-base titrations, centrifugation, and solids washing[29]. Compositional analysis details for the resulting extract are provided in *SI Appendix*, Table S1[150].

Yeast Strain, medium Summary, and cultivation

Cutaneotrichosporon oleaginosum ATCC 20,509 (formerly classified as *Cryptococcus curvatus*) was used in this study. For long-term storage, glycerol (15% v/v) stocks stored at − 80 °C were prepared from cells streaked on standard Yeast extract-Peptone-Dextrose (YPD) plates. YPD was used for short term plate storage at 4 °C as well as generating seed cultures. The yeast was cultivated in a YNB-based experimental medium containing 1 g/L carbon source (lignin extract, glucose, or benzoate) or no additional carbon source ("No Carbon" condition). Cultivation conditions were 28 °C shaking at 180 rpm.

2D-HSQC-NMR
Two-dimensional (2D) heteronuclear single-quantum correlation (HSQC) NMR spectroscopy was used to compare alkali lignin (time-matched control) to lignin in the lyophilized yeast culture supernatants[151,152].

Fluorescence microscopy
Live yeast cultures were imaged by an inverted fluorescence confocal microscope with oil immersion. The fluorescence from lignin was excited by a 488 nm wavelength laser according to a preliminary analysis of lignin excitation and emission wavelengths (SI Appendix, Fig. S5). The Cellpose software was employed for cellular segmentation to analyze yeast cell fluorescence for the aforementioned carbon source conditions.

Secretomics and cellular proteomics
Supernatants and washed pellets were collected from yeast cultivations to generate extracellular (secretomics) and intracellular (cellular proteomics) samples, respectively. All samples were processed using the SP3 method as described before[153] but with modifications depending on the sample type (Fig. 1)[154,155]. All samples were digested with an enzyme cocktail containing trypsin (Promega) and Lys-C (Wako Chemicals). Samples were then processed with Zip-Tip C18 SPE and analyzed using LC-MS/MS.

Data analysis and processing
Two-tailed *t*-tests were used for determining statistically significant differences in growth, total aromatics, and fluorescence intensities among conditions. For these analyses, *p*-values were adjusted for multiple comparisons using the Holm's method. Significance levels and error bars are defined in each figure caption. Protein sequences and annotations for *C. oleaginosum* were retrieved from the respective Joint Genome Institute (JGI) database[91,130]. Bottom-up proteomics data were processed with MaxQuant for label-free quantification[156]. All $\log_2$ foldchange ("FC") data corresponds to differential expression analysis using the DEqMS package with MaxQuant LFQ intensities, unless otherwise specified as using the DEP package with normalized raw intensity values (*SI Appendix*, Datasets S1–2)[157,158]. For proteomics differential expression analysis, *p*-values were adjusted using the the Benjamini–Hochberg procedure. Refer to *SI Appendix*, Supplementary Methods for details regarding RStudio Bioconductor packages and annotation prediction tools used for bioinformatics analyses[159]. Proteins were considered homologous when BLASTp hits exhibited ≥ 30% identity and ≥ 30% coverage with an e-value ≤ 1e-10. A permissive coverage threshold was chosen to include cases where conserved catalytic domains are present. All unfiltered BLASTp results are provided in *SI Appendix*, Dataset S3.

Data availability
The datasets used and/or analysed during the current study are included in the main text and supplementary materials or available from the corresponding author on reasonable request. All mass spectrometry proteomics data generated for this study have been deposited in the MassIVE repository, a full member of the ProteomeXchange consortium. The datasets can be accessed using the identifier MSV000095797 after logging in using the username (MSV000095797) and password (Yeast5963). Additional data are available in the SI Appendix and Datasets S1–S4.

Received: 29 March 2025; Accepted: 13 January 2026
Published online: 18 January 2026

References
1. Wang, H., Pu, Y., Ragauskas, A. & Yang, B. From lignin to valuable products–strategies, challenges, and prospects. *Bioresour Technol.* **271**, 449–461 (2019).
2. Grgas, D. et al. The bacterial degradation of Lignin—A review. *Water* **15**, 1272 (2023).
3. Davis, R. E. et al. Process design and economics for the conversion of lignocellulosic biomass to hydrocarbon fuels and coproducts: 2018 biochemical design case Update; biochemical Deconstruction and conversion of biomass to fuels and products via integrated biorefinery pathways (2018). National Renewable Energy Laboratory, Golden, CO. NREL/TP-5100-71949.
4. Sale, K. et al. Synthetic Microbial Consortium for Biological Breakdown and Conversion of Lignin Sandia National Laboratories, Albuquerque, NM. SAND2022-131. (2022).
5. Saini, S. & Sharma, K. K. Fungal lignocellulolytic enzymes and lignocellulose: A critical review on their contribution to multiproduct biorefinery and global biofuel research. *Int. J. Biol. Macromol.* **193**, 2304–2319 (2021).
6. Granja-Travez, R. S., Persinoti, G. F., Squina, F. M. & Bugg, T. D. H. Functional genomic analysis of bacterial lignin degraders: diversity in mechanisms of lignin oxidation and metabolism. *Appl. Microbiol. Biotechnol.* **104**, 3305–3320 (2020).
7. Schick Zapanta, L. & Tien, M. The roles of Veratryl alcohol and oxalate in fungal lignin degradation. *J. Biotechnol.* **53**, 93–102 (1997).
8. Shin, S. K., Ko, Y. J., Hyeon, J. E. & Han, S. O. Studies of advanced lignin valorization based on various types of lignolytic enzymes and microbes. *Bioresour Technol.* **289**, 121728 (2019).
9. Janusz, G. et al. Lignin degradation: microorganisms, enzymes involved, genomes analysis and evolution. *FEMS Microbiol. Rev.* **41**, 941–962 (2017).
10. Brink, D. P., Ravi, K., Lidén, G. & Gorwa-Grauslund, M. F. Mapping the diversity of microbial lignin catabolism: experiences from the eLignin database. *Appl. Microbiol. Biotechnol.* **103**, 3979–4002 (2019).
11. Hainal, A. R., Capraru, A. M., Volf, I. & Popa, V. I. Lignin as a carbon source for the cultivation of some *Rhodotorula* species. *Cellul Chem. Technol* 87–96 (2012).
12. Sláviková, E. & Košíková, B. Modification of lignin by *Geotrichum Klebahnii*. *World J. Microbiol. Biotechnol.* **17**, 1–3 (2001).
13. Sláviková, E., Košíková, B. & Mikulášová, M. Biotransformation of waste lignin products by the soil-inhabiting yeast *Trichosporon pullulans*. *Can. J. Microbiol.* **48**, 200–203 (2002).
14. Broos, W. et al. Evaluation of lignocellulosic wastewater valorization with the oleaginous yeasts *R. kratochvilovae* EXF7516 and *C. oleaginosum* ATCC 20509. *Fermentation* **8**, 204 (2022).
15. Wakil, S. et al. Production, characterization and purification of laccase by yeasts isolated from ligninolytic soil. *J. Pure Appl. Microbiol.* **11**, 847–869 (2017).

16. Ali, S. S. et al. Coupling Azo dye degradation and biodiesel production by manganese-dependent peroxidase producing oleaginous yeasts isolated from wood-feeding termite gut symbionts. *Biotechnol. Biofuels*. **14**, 61 (2021).
17. Ali, S. S., Al-Tohamy, R. & Sun, J. Performance of *Meyerozyma caribbica* as a novel manganese peroxidase-producing yeast inhabiting wood-feeding termite gut symbionts for Azo dye decolorization and detoxification. *Sci. Total Environ.* **806**, 150665 (2022).
18. Ai, M., Zhu, Y. & Jia, X. Recent advances in constructing artificial microbial consortia for the production of medium-chain-length polyhydroxyalkanoates. *World J. Microbiol. Biotechnol.* **37**, 2 (2021).
19. Braun, M. K. et al. Catalytic decomposition of the oleaginous yeast *Cutaneotrichosporon oleaginosus* and subsequent biocatalytic conversion of liberated free fatty acids. *ACS Sustain. Chem. Eng.* **7**, 6531–6540 (2019).
20. Sawpan, M. A. Polyurethanes from vegetable oils and applications: a review. *J. Polym. Res.* **25**, 184 (2018).
21. Patel, A. et al. An overview of potential oleaginous microorganisms and their role in biodiesel and Omega-3 fatty acid-based industries. *Microorganisms* 8, (2020).
22. Yaguchi, A., Robinson, A., Mihealsick, E. & Blenner, M. Metabolism of aromatics by *Trichosporon oleaginosus* while remaining oleaginous. *Microb. Cell. Factories*. **16**, 206 (2017).
23. Bracharz, F., Beukhout, T., Mehlmer, N. & Brück, T. Opportunities and challenges in the development of *Cutaneotrichosporon oleaginosus* ATCC 20509 as a new cell factory for custom tailored microbial oils. *Microb. Cell. Factories*. **16**, 178 (2017).
24. Yaguchi, A., Rives, D. & Blenner, M. New kids on the block: emerging oleaginous yeast of biotechnological importance. *AIMS Microbiol.* **3**, 227–247 (2017).
25. Yaguchi, A. *Development of Cutaneotrichosporon Oleaginosus To Convert Lignin-Derived Phenolics To Oleochemicals* (Clemson University, 2020).
26. Li, X., Li, M., Pu, Y., Ragauskas, A. J. & Zheng, Y. Black liquor valorization by using marine protist *Thraustochytrium striatum* and the preliminary metabolic mechanism study. *ACS Sustain. Chem. Eng.* **8**, 1786–1796 (2020).
27. Wang, W., Chen, X., Katahira, R. & Tucker, M. Characterization and Deconstruction of oligosaccharides in black liquor from deacetylation process of corn Stover. *Front. Energy Res.* **7**, 54 (2019).
28. Vilela, N. et al. Integrative omics analyses of the ligninolytic *Rhodosporidium fluviale* LM-2 disclose catabolic pathways for biobased chemical production. *Biotechnol. Biofuels Bioprod.* **16**, 5 (2023).
29. He, Y., Li, X., Ben, H., Xue, X. & Yang, B. Lipid production from dilute alkali corn Stover lignin by *Rhodococcus* strains. *ACS Sustain. Chem. Eng.* **5**, 2302–2311 (2017).
30. Vermaas, J. V. et al. Passive membrane transport of lignin-related compounds. *Proc. Natl. Acad. Sci.* **116**, 23117–23123 (2019).
31. Fujita, M. et al. A TonB-dependent receptor constitutes the outer membrane transport system for a lignin-derived aromatic compound. *Commun. Biol.* **2**, 1–10 (2019).
32. Beckham, G. T., Johnson, C. W., Karp, E. M., Salvachúa, D. & Vardon, D. R. Opportunities and challenges in biological lignin valorization. *Curr. Opin. Biotechnol.* **42**, 40–53 (2016).
33. Michalska, K. et al. Characterization of transport proteins for aromatic compounds derived from lignin: benzoate derivative binding proteins. *J. Mol. Biol.* **423**, 555–575 (2012).
34. Ozbek, O. & Ulgen, O. Ileri Ercan, N. The toxicity of Polystyrene-Based nanoparticles in *Saccharomyces cerevisiae* is associated with nanoparticle charge and uptake mechanism. *Chem. Res. Toxicol.* **34**, 1055–1068 (2021).
35. Baldacci-Cresp, F. et al. A rapid and quantitative safranin-based fluorescent microscopy method to evaluate cell wall lignification. *Plant. J.* **102**, 1074–1089 (2020).
36. Hawkins, S. & Boudet, A. Wound-induced lignin and Suberin deposition in a Woody angiosperm (*Eucalyptus Gunnii* Hook.): histochemistry of early changes in young plants. *Protoplasma* **191**, 96–104 (1996).
37. Gill, C. O., Hall, M. J. & Ratledge, C. Lipid accumulation in an oleaginous yeast (*Candida* 107) growing on glucose in single-stage continuous culture. *Appl. Environ. Microbiol.* **33**, 231–239 (1977).
38. Hansson, L. & Dostálek, M. Lipid formation by *Cryptococcus albidus* in nitrogen-limited and in carbon-limited Chemostat cultures. *Appl. Microbiol. Biotechnol.* **24**, 187–192 (1986).
39. Lankiewicz, T. S. et al. Lignin Deconstruction by anaerobic fungi. *Nat. Microbiol.* **8**, 596–610 (2023).
40. Chua, M. G. S., Chen, C. L., Chang, H. M. & Kirk, T. K. 13 C NMR Spectroscopic Study of Spruce Lignin Degraded *Phanerochaete chrysosporium*. *Holzforschung* **36**, 165–172 (1982).
41. Yelle, D. J., Wei, D., Ralph, J. & Hammel, K. E. Multidimensional NMR analysis reveals truncated lignin structures in wood decayed by the brown rot basidiomycete *Postia placenta*. *Environ. Microbiol.* **13**, 1091–1100 (2011).
42. Oates, N. C. et al. A multi-omics approach to lignocellulolytic enzyme discovery reveals a new ligninase activity from *Parascedosporium putredinis* NO1. *Proc. Natl. Acad. Sci.* **118**, e2008888118 (2021).
43. Awad, D. & Brueck, T. Optimization of protein isolation by proteomic qualification from *Cutaneotrichosporon oleaginosus*. *Anal. Bioanal Chem.* **412**, 449–462 (2020).
44. Fuchs, T. et al. Identifying carbohydrate-active enzymes of *Cutaneotrichosporon oleaginosus* using systems biology. *Microb. Cell. Factories*. **20**, 205 (2021).
45. Teufel, F. et al. SignalP 6.0 predicts all five types of signal peptides using protein Language models. *Nat. Biotechnol.* **40**, 1023–1025 (2022).
46. Barrett, K., Hunt, C. J., Lange, L. & Meyer, A. S. Conserved unique peptide patterns (CUPP) online platform: peptide-based functional annotation of carbohydrate active enzymes. *Nucleic Acids Res.* **48**, W110–W115 (2020).
47. Pócsi, I., Prade, R. A., Penninckx, M. J. & Glutathione Altruistic Metabolite in Fungi. in *Advances in Microbial Physiology* **49** 1–76 (Academic Press, 2004).
48. Goodell, B. et al. Low molecular weight chelators and phenolic compounds isolated from wood decay fungi and their role in the fungal biodegradation of wood. *J. Biotechnol.* **53**, 133–162 (1997).
49. Hammel, K. E., Kapich, A. N., Jensen, K. A. & Ryan, Z. C. Reactive oxygen species as agents of wood decay by fungi. *Enzyme Microb. Technol.* **30**, 445–453 (2002).
50. Arantes, V., Milagres, A. M. F., Filley, T. R. & Goodell, B. Lignocellulosic polysaccharides and lignin degradation by wood decay fungi: the relevance of nonenzymatic Fenton-based reactions. *J. Ind. Microbiol. Biotechnol.* **38**, 541–555 (2011).
51. Mattila, H., Österman-Udd, J., Mali, T. & Lundell, T. Basidiomycota fungi and ROS: genomic perspective on key enzymes involved in generation and mitigation of reactive oxygen species. *Front. Fungal Biol.* **3**, 837605 (2022).
52. Drula, E. et al. The carbohydrate-active enzyme database: functions and literature. *Nucleic Acids Res.* **50**, D571–D577 (2022).
53. Thurston, C. F. The structure and function of fungal laccases. *Microbiology* **140**, 19–26 (1994).
54. Glumoff, T. et al. Lignin peroxidase from *Phanerochaete-chrysosporium*. *Eur. J. Biochem.* **187**, 515–520 (1990).
55. Jensen, K. A., Houtman, C. J., Ryan, Z. C. & Hammel, K. E. Pathways for extracellular Fenton chemistry in the brown rot basidiomycete *Gloeophyllum trabeum*. *Appl. Environ. Microbiol.* **67**, 2705–2711 (2001).
56. Arantes, V. & Goodell, B. Current Understanding of Brown-Rot fungal biodegradation mechanisms: A review in Deterioration and Protection of Sustainable Biomaterials, (eds Schultz, T. P., Goodell, B. & Nicholas, D. D.) (American Chemical Society, 3–21. (2014).
57. Krueger, M. C., Bergmann, M. & Schlosser, D. Widespread ability of fungi to drive Quinone redox cycling for biodegradation. *FEMS Microbiol. Lett.* **363**, fnw105 (2016).
58. Guillén, F., Martínez, M. J., Muñoz, C. & Martínez, A. T. Quinone redox cycling in the ligninolytic fungus *Pleurotus eryngii* leading to extracellular production of superoxide anion radical. *Arch. Biochem. Biophys.* **339**, 190–199 (1997).

59. Prousek, J. Fenton chemistry in biology and medicine. *Pure Appl. Chem.* **79**, 2325–2338 (2007).
60. Camacho, C. et al. BLAST+: architecture and applications. *BMC Bioinform.* **10**, 421 (2009).
61. Dancis, A., Roman, D. G., Anderson, G. J., Hinnebusch, A. G. & Klausner, R. D. Ferric reductase of Saccharomyces cerevisiae: molecular characterization, role in iron uptake, and transcriptional control by iron. *Proc. Natl. Acad. Sci. U S A.* **89**, 3869–3873 (1992).
62. Goodell, B., Qian, Y. & Jellison, J. Fungal decay of wood: soft rot—Brown rot—White rot in Development of Commercial Wood Preservatives, (eds Schultz, T. P., Militz, H., Freeman, M. H., Goodell, B. & Nicholas, D. D.) (American Chemical Society, 9–31. (2008).
63. Philpott, C. C. Iron uptake in fungi: A system for every source. *Biochim. Biophys. Acta BBA - Mol. Cell. Res.* **1763**, 636–645 (2006).
64. Zhang, J., Silverstein, K. A. T., Castaño, J. D., Figueroa, M. & Schilling, J. S. Gene regulation shifts shed light on fungal adaption in plant biomass decomposers. *mBio* **10**, e02176–e02119 (2019).
65. Castaño, J. D., Khoury, E., Goering, I. V., Evans, J., Zhang, J. & J. E. & Unlocking the distinctive enzymatic functions of the early plant biomass deconstructive genes in a brown rot fungus by cell-free protein expression. *Appl. Environ. Microbiol.* **90**, e00122–e00124 (2024).
66. Paysan-Lafosse, T. et al. InterPro in 2022. *Nucleic Acids Res.* **51**, D418–D427 (2023).
67. Liu, J. et al. An extracellular Zn-only superoxide dismutase from *Puccinia striiformis* confers enhanced resistance to host-derived oxidative stress. *Environ. Microbiol.* **18**, 4118–4135 (2016).
68. Jiang, Y. et al. MULocDeep: A deep-learning framework for protein subcellular and suborganellar localization prediction with residue-level interpretation. *Comput. Struct. Biotechnol. J.* **19**, 4825–4839 (2021).
69. Sützl, L., Foley, G., Gillam, E. M. J., Bodén, M. & Haltrich, D. The GMC superfamily of oxidoreductases revisited: analysis and evolution of fungal GMC oxidoreductases. *Biotechnol. Biofuels.* **12**, 118 (2019).
70. Kersten, P. & Cullen, D. Copper radical oxidases and related extracellular oxidoreductases of wood-decay agaricomycetes. *Fungal Genet. Biol.* **72**, 124–130 (2014).
71. Escutia, M. R. et al. Cloning and sequencing of two *Ceriporiopsis subvermispora* Bicupin oxalate oxidase allelic isoforms: implications for the reaction specificity of oxalate oxidases and decarboxylases. *Appl. Environ. Microbiol.* **71**, 3608–3616 (2005).
72. Presley, G. N., Zhang, J. & Schilling, J. S. A genomics-informed study of oxalate and cellulase regulation by brown rot wood-degrading fungi. *Fungal Genet. Biol.* **112**, 64–70 (2018).
73. Yaropolov, A. I., Skorobogat'ko, O. V., Vartanov, S. S., Varfolomeyev, S. D. & Laccase *Appl. Biochem. Biotechnol.* **49**, 257–280 (1994).
74. Ong, E., Pollock, W. B. R. & Smith, M. Cloning and sequence analysis of two laccase complementary DNAs from the ligninolytic basidiomycete *Trametes versicolor*. *Gene* **196**, 113–119 (1997).
75. Levasseur, A., Drula, E., Lombard, V., Coutinho, P. M. & Henrissat, B. Expansion of the enzymatic repertoire of the CAZy database to integrate auxiliary redox enzymes. *Biotechnol. Biofuels.* **6**, 41 (2013).
76. Kersten, P. & Cullen, D. Extracellular oxidative systems of the lignin-degrading basidiomycete *Phanerochaete Chrysosporium*. *Fungal Genet. Biol.* **44**, 77–87 (2007).
77. Jönsson, L., Sjöström, K., Häggström, I. & Nyman, P. O. Characterization of a laccase gene from the white-rot fungus *Trametes versicolor* and structural features of basidiomycete laccases. *Biochim. Biophys. Acta BBA - Protein Struct. Mol. Enzymol.* **1251**, 210–215 (1995).
78. Larrondo, L. F., Canessa, P., Melo, F., Polanco, R. & Vicuña, R. Cloning and characterization of the genes encoding the high-affinity iron-uptake protein complex Fet3/Ftr1 in the basidiomycete *Phanerochaete Chrysosporium*. *Microbiology* **153**, 1772–1780 (2007).
79. Kües, U. & Rühl, M. Multiple Multi-Copper oxidase gene families in Basidiomycetes – What for? *Curr. Genomics.* **12**, 72–94 (2011).
80. Cantalapiedra, C. P., Hernández-Plaza, A., Letunic, I., Bork, P. & Huerta-Cepas J. eggNOG-mapper v2: functional Annotation, orthology Assignments, and domain prediction at the metagenomic scale. *Mol. Biol. Evol.* **38**, 5825–5829 (2021).
81. Akileswaran, L., Brock, B. J., Cereghino, J. L. & Gold, M. H. 1,4-Benzoquinone reductase from *Phanerochaete chrysosporium*: cDNA cloning and regulation of expression. *Appl. Environ. Microbiol.* **65**, 415–421 (1999).
82. Brock, B. J., Rieble, S. & Gold, M. H. Purification and characterization of a 1,4-Benzoquinone reductase from the basidiomycete *Phanerochaete Chrysosporium*. *Appl. Environ. Microbiol.* **61**, 3076–3081 (1995).
83. Brock, B. J. & Gold, M. H. 1,4-Benzoquinone reductase from the basidiomycete *Phanerochaete chrysosporium*: spectral and kinetic analysis. *Arch. Biochem. Biophys.* **331**, 31–40 (1996).
84. Jensen, K. A., Ryan, Z. C., Wymelenberg, V., Cullen, A., Hammel, K. E. & D. & An nadh:quinone oxidoreductase active during biodegradation by the Brown-Rot basidiomycete *Gloeophyllum trabeum*. *Appl. Environ. Microbiol.* **68**, 2699–2703 (2002).
85. Wang, J. et al. The conserved domain database in 2023. *Nucleic Acids Res.* **51**, D384–D388 (2023).
86. Kawai, S., Umezawa, T. & Higuchi, T. -Benzoquinone monoketals, novel degradation products of β-*O*-4 lignin model compounds by *Coriolus versicolor* and lignin peroxidase of *Phanerochaete Chrysosporium*. *FEBS Lett.* **210**, 61–65 (1987).
87. Adnan, M. et al. Carbon catabolite repression in filamentous fungi. *Int. J. Mol. Sci.* **19**, 48 (2017).
88. Martínez, M. J., Ruiz-Dueñas, F. J., Guillén, F. & Martínez, Á. T. Purification and catalytic properties of two manganese peroxidase isoenzymes from *Pleurotus eryngii*. *Eur. J. Biochem.* **237**, 424–432 (1996).
89. Martorell, M. M., Pajot, H. F. & Figueroa, L. I. C. D. Biological degradation of reactive black 5 dye by yeast *Trichosporon Akiyoshidainum*. *J. Environ. Chem. Eng.* **5**, 5987–5993 (2017).
90. Kobayashi, Y. et al. Chromosome-level genome assemblies of *Cutaneotrichosporon* spp. (Trichosporonales, Basidiomycota) reveal imbalanced evolution between nucleotide sequences and chromosome synteny. *BMC Genom.* **24**, 609 (2023).
91. Close, D. & Ojumu, J. Draft genome sequence of the oleaginous yeast *Cryptococcus curvatus* ATCC 20509. *Genome Announc.* **4**, e01235–e01216 (2016).
92. Grigoriev, I. V. et al. The genome portal of the department of energy joint genome Institute. *Nucleic Acids Res.* **40**, D26–D32 (2012).
93. Twala, P. P., Mitema, A., Baburam, C. & Feto, N. A. Breakthroughs in the discovery and use of different peroxidase isoforms of microbial origin. *AIMS Microbiol.* **6**, 330–349 (2020).
94. Paszczynski, A., Crawford, R., Funk, D. & Goodell, B. De Novo synthesis of 4,5-Dimethoxycatechol and 2,5-Dimethoxyhydroquinone by the brown rot fungus *Gloeophyllum trabeum*. *Appl. Environ. Microbiol.* **65**, 674–679 (1999).
95. Chiang, Y. M., Lin, T. S. & Wang, C. C. C. Total heterologous biosynthesis of fungal natural products in *Aspergillus Nidulans*. *J. Nat. Prod.* **85**, 2484–2518 (2022).
96. Sha, Y. et al. Adaptive laboratory evolution boosts *Yarrowia lipolytica* tolerance to vanillic acid. *J. Biotechnol.* **367**, 42–52 (2023).
97. Barnhart-Dailey, M. C. et al. Internalization and accumulation of model lignin breakdown products in bacteria and fungi. *Biotechnol. Biofuels.* **12**, 175 (2019).
98. Shimizu, M., Kobayashi, Y., Tanaka, H. & Wariishi, H. Transportation mechanism for Vanillin uptake through fungal plasma membrane. *Appl. Microbiol. Biotechnol.* **68**, 673–679 (2005).
99. Saier, M. H. Jr et al. The transporter classification database (TCDB): 2021 update. *Nucleic Acids Res.* **49**, D461–D467 (2021).
100. Chen, J. Y., Kuruparan, A., Zamani-Babgohari, M. & Gonzales-Vigil, E. Dynamic changes to the plant cuticle include the production of volatile cuticular wax–derived compounds. *Proc. Natl. Acad. Sci.* **120**, e2307012120 (2023).
101. Cillingová, A. et al. Eukaryotic transporters for hydroxyderivatives of benzoic acid. *Sci. Rep.* **7**, 8998 (2017).

102. Nomura, T. et al. Exposure of the yeast *Saccharomyces cerevisiae* to functionalized polystyrene latex nanoparticles: influence of surface charge on toxicity. *Environ. Sci. Technol.* **47**, 3417–3423 (2013).
103. Nomura, T., Kuriyama, Y., Toyoda, S. & Konishi, Y. Direct measurements of colloidal behavior of polystyrene nanoparticles into budding yeast cells using atomic force microscopy and confocal microscopy. *Colloids Surf. Physicochem Eng. Asp*. **555**, 653–659 (2018).
104. Maslanka, R., Kwolek-Mirek, M. & Zadrag-Tecza, R. Autofluorescence of yeast *Saccharomyces cerevisiae* cells caused by glucose metabolism products and its methodological implications. *J. Microbiol. Methods*. **146**, 55–60 (2018).
105. Bhatta, H. & Goldys, E. M. Characterization of yeast strains by fluorescence lifetime imaging microscopy. *FEMS Yeast Res.* **8**, 81–87 (2008).
106. Stringer, C., Wang, T., Michaelos, M. & Pachitariu, M. Cellpose: a generalist algorithm for cellular segmentation. *Nat. Methods*. **18**, 100–106 (2021).
107. Surre, J. et al. Strong increase in the autofluorescence of cells signals struggle for survival. *Sci. Rep.* **8**, 12088 (2018).
108. Hazan, R., Levine, A. & Abeliovich, H. Benzoic acid, a weak organic acid food Preservative, exerts specific effects on intracellular membrane trafficking pathways in *Saccharomyces cerevisiae*. *Appl. Environ. Microbiol.* **70**, 4449–4457 (2004).
109. Awashra, M. & Młynarz, P. The toxicity of nanoparticles and their interaction with cells: an in vitro metabolomic perspective. *Nanoscale Adv.* **5**, 2674–2723 (2023).
110. Ali, S. S. et al. Could termites be hiding a goldmine of obscure yet promising yeasts for energy crisis solutions based on aromatic wastes? A critical state-of-the-art review. *Biotechnol. Biofuels Bioprod.* **15**, 35 (2022).
111. Ahuatzi-chacón, D. et al. Kinetic study of phenol hydroxylase and catechol 1,2-dioxygenase biosynthesis by *Candida tropicalis* cells grown on different phenolic substrates. *World J. Microbiol. Biotechnol.* **20**, 695–702 (2004).
112. Durham, D. R., McNamee, C. G. & Stewart, D. B. Dissimilation of aromatic compounds in *Rhodotorula graminis*: biochemical characterization of pleiotropically negative mutants. *J. Bacteriol.* **160**, 771–777 (1984).
113. Anderson, E. M. et al. Reductive catalytic fractionation of corn Stover lignin. *ACS Sustain. Chem. Eng.* **4**, 6940–6950 (2016).
114. Broos, W. et al. *Rhodotorula Kratochvilovae* outperforms *Cutaneotrichosporon oleaginosum* in the valorisation of lignocellulosic wastewater to microbial oil. *Process. Biochem.* **137**, 229–238 (2024).
115. Yaguchi, A. et al. Identification of oleaginous yeasts that metabolize aromatic compounds. *J. Ind. Microbiol. Biotechnol.* **47**, 801–813 (2020).
116. Nogué, V. S. et al. Integrated diesel production from lignocellulosic sugars via oleaginous yeast. *Green. Chem.* **20**, 4349–4365 (2018).
117. Sachan, A., Ghosh, S. & Mitra, A. Biotransformation of *p*-coumaric acid by *Paecilomyces variotii*. *Lett. Appl. Microbiol.* **42**, 35–41 (2006).
118. Sachan, A., Ghosh, S. & Mitra, A. Transforming *p*-coumaric acid into *p*-hydroxybenzoic acid by the mycelial culture of a white rot fungus. *Afr. J. Microbiol. Res.* **4**, 267–273 (2009).
119. Lubbers, R. J. M. et al. Discovery of novel *p*-Hydroxybenzoate-*m*-hydroxylase, Protocatechuate 3,4 Ring-Cleavage dioxygenase, and hydroxyquinol 1,2 Ring-Cleavage dioxygenase from the filamentous fungus *Aspergillus Niger*. *ACS Sustain. Chem. Eng.* **7**, 19081–19089 (2019).
120. Lubbers, R. J. M. et al. Evolutionary adaptation of *Aspergillus Niger* for increased ferulic acid tolerance. *J. Appl. Microbiol.* **128**, 735–746 (2020).
121. Lubbers, R. J. M., Dilokpimol, A., Visser, J. & de Vries, R. P. *Aspergillus Niger* uses the peroxisomal CoA-dependent β-oxidative genes to degrade the hydroxycinnamic acids caffeic acid, ferulic acid, and *p*-coumaric acid. *Appl. Microbiol. Biotechnol.* **105**, 4199–4211 (2021).
122. Gallage, N. J. & Møller, B. L. Vanillin–Bioconversion and bioengineering of the most popular plant flavor and its *De Novo* biosynthesis in the vanilla Orchid. *Mol. Plant.* **8**, 40–57 (2015).
123. Fleige, C., Hansen, G., Kroll, J. & Steinbüchel, A. Investigation of the *Amycolatopsis* sp. Strain ATCC 39116 Vanillin dehydrogenase and its impact on the biotechnical production of Vanillin. *Appl. Environ. Microbiol.* **79**, 81–90 (2013).
124. Achterholt, S., Priefert, H. & Steinbüchel, A. Identification of *Amycolatopsis* sp. strain HR167 genes, involved in the bioconversion of ferulic acid to Vanillin. *Appl. Microbiol. Biotechnol.* **54**, 799–807 (2000).
125. Mitra, A. et al. 4-Hydroxycinnamoyl-CoA Hydratase/lyase (HCHL)—An enzyme of phenylpropanoid chain cleavage from *Pseudomonas*. *Arch. Biochem. Biophys.* **365**, 10–16 (1999).
126. Neuberger, G., Maurer-Stroh, S., Eisenhaber, B., Hartig, A. & Eisenhaber, F. Prediction of peroxisomal targeting signal 1 containing proteins from amino acid sequence. *J. Mol. Biol.* **328**, 581–592 (2003).
127. Thumuluri, V., Almagro Armenteros, J. J., Johansen, A. R., Nielsen, H. & Winther, O. DeepLoc 2.0: multi-label subcellular localization prediction using protein Language models. *Nucleic Acids Res.* **50**, W228–W234 (2022).
128. Neujahr, H. Y. & Gaal, A. Phenol hydroxylase from yeast: sulfhydryl groups in phenol hydroxylase from *Trichosporon cutaneum*. *Eur. J. Biochem.* **58**, 351–357 (1975).
129. Kalin, M., Neujahr, H. Y., Weissmahr, R. N., Sejlitz, T. & Reiser, J. Phenol hydroxylase from *Trichosporon cutaneum*: gene Cloning, sequence Analysis, and functional expression in *Eschenichia coli*. *J. Bacteriol.* **174**, 7112–7120 (1992).
130. Nordberg, H. et al. The genome portal of the department of energy joint genome institute: 2014 updates. *Nucleic Acids Res.* **42**, D26–D31 (2014).
131. Westphal, A. H., Tischler, D. & van Berkel, W. J. H. Natural diversity of FAD-dependent 4-hydroxybenzoate hydroxylases. *Arch. Biochem. Biophys.* **702**, 108820 (2021).
132. del Cerro, C. et al. Intracellular pathways for lignin catabolism in white-rot fungi. *Proc. Natl. Acad. Sci.* **118**, e2017381118 (2021).
133. Holesova, Z. et al. Gentisate and 3-oxoadipate pathways in the yeast *Candida parapsilosis*: identification and functional analysis of the genes coding for 3-hydroxybenzoate 6-hydroxylase and 4-hydroxybenzoate 1-hydroxylase. *Microbiology* **157**, 2152–2163 (2011).
134. Degradation of Homocyclic Aromatic Compounds by Fungi in. in *Encyclopedia of Mycology*. 477–488 (eds Zaragoza, Ó. & Casadevall, A.) (Elsevier, 2021).
135. Semana, P. & Powlowski, J. Four aromatic intradiol ring cleavage dioxygenases from *Aspergillus Niger*. *Appl. Environ. Microbiol.* **85**, e01786–e01719 (2019).
136. Lubbers, R. J. M. et al. Vanillic acid and methoxyhydroquinone production from guaiacyl units and related aromatic compounds using Aspergillus Niger cell factories. *Microb. Cell. Factories*. **20**, 151 (2021).
137. Cillingová, A. et al. Transcriptome and proteome profiling reveals complex adaptations of *Candida parapsilosis* cells assimilating hydroxyaromatic carbon sources. *PLOS Genet.* **18**, e1009815 (2022).
138. Skrzypek, M. S. et al. The *Candida* genome database (CGD): incorporation of assembly 22, systematic identifiers and visualization of high throughput sequencing data. *Nucleic Acids Res.* **45**, D592–D596 (2017).
139. Mazur, P. et al. *Cis,cis*-Muconate lactonizing enzyme from *Trichosporon cutaneum*: evidence for a novel class of cycloisomerases in eucaryotes. *Biochemistry* **33**, 1961–1970 (1994).
140. Martins, T. M. et al. The old 3-oxoadipate pathway revisited: new insights in the catabolism of aromatics in the saprophytic fungus *Aspergillus Nidulans*. *Fungal Genet. Biol.* **74**, 32–44 (2015).
141. Hibi, M., Sonoki, T. & Mori, H. Functional coupling between vanillate-*O*-demethylase and formaldehyde detoxification pathway. *FEMS Microbiol. Lett.* **253**, 237–242 (2005).

142. Veličković, M. et al. Mapping microhabitats of lignocellulose decomposition by a microbial consortium. *Nat. Chem. Biol.* **20**, 1033–1043 (2024).
143. Perna, V. et al. Laccase-Catalyzed oxidation of lignin induces production of H_2O_2. *ACS Sustain. Chem. Eng.* **8**, 831–841 (2020).
144. Li, X., Gluth, A., Zhang, T. & Qian, W. J. Thiol redox proteomics: characterization of thiol-based post-translational modifications. *PROTEOMICS* **23**, 2200194 (2023).
145. Li, X., Gluth, A., Feng, S., Qian, W. J. & Yang, B. Harnessing redox proteomics to study metabolic regulation and stress response in lignin-fed *Rhodococci*. *Biotechnol. Biofuels Bioprod.* **16**, 180 (2023).
146. Kourist, R. et al. Genomics and transcriptomics analyses of the Oil-Accumulating basidiomycete yeast trichosporon oleaginosus: insights into substrate utilization and alternative evolutionary trajectories of fungal mating systems. *mBio* **6**, e00918–e00915 (2015).
147. Zhu, X. & Williamson, P. R. Role of laccase in the biology and virulence of *Cryptococcus neoformans*. *FEMS Yeast Res.* **5**, 1–10 (2004).
148. Chen, X. et al. The impacts of deacetylation prior to dilute acid pretreatment on the bioethanol process. *Biotechnol. Biofuels*. **5**, 8 (2012).
149. Chen, X. et al. A highly efficient dilute alkali deacetylation and mechanical (disc) refining process for the conversion of renewable biomass to lower cost sugars. *Biotechnol. Biofuels*. **7**, 98 (2014).
150. Sluiter, A. et al. Determination of Structural Carbohydrates and Lignin in Biomass National Renewable Energy Laboratory, Bolder, CO. NREL/TP-510-42618. (2012).
151. Li, X., Li, M., Pu, Y., Ragauskas, A. J. & Zheng, Y. Simultaneous depolymerization and fermentation of lignin into value-added products by the marine protist, *Thraustochytrium striatum*. *Algal Res.* **46**, 101773 (2020).
152. Li, X. et al. Inhibitory effects of lignin on enzymatic hydrolysis: the role of lignin chemistry and molecular weight. *Renew. Energy*. **123**, 664–674 (2018).
153. Gluth, A. et al. Nitrogen limitation causes a seismic shift in redox state and phosphorylation of proteins implicated in carbon flux and lipidome remodeling in *Rhodotorula toruloides*. *Biotechnol. Biofuels Bioprod.* **18**, 80 (2025).
154. Hughes, C. S. et al. Single-pot, solid-phase-enhanced sample Preparation for proteomics experiments. *Nat. Protoc.* **14**, 68–85 (2019).
155. Hughes, C. S. et al. Ultrasensitive proteome analysis using paramagnetic bead technology. *Mol. Syst. Biol.* **10**, 757 (2014).
156. Cox, J. et al. Accurate Proteome-wide Label-free quantification by delayed normalization and maximal peptide ratio Extraction, termed MaxLFQ. *Mol. Cell. Proteom. MCP*. **13**, 2513–2526 (2014).
157. Zhu, Y. et al. DEqMS: A method for accurate variance Estimation in differential protein expression Analysis *. *Mol. Cell. Proteom.* **19**, 1047–1057 (2020).
158. Zhang, X. et al. Proteome-wide identification of ubiquitin interactions using UbIA-MS. *Nat. Protoc.* **13**, 530–550 (2018).
159. Huber, W. et al. Orchestrating high-throughput genomic analysis with bioconductor. *Nat. Methods*. **12**, 115–121 (2015).
160. Smeekens, J. M., Xiao, H. & Wu, R. Global analysis of secreted proteins and glycoproteins in *Saccharomyces cerevisiae*. *J. Proteome Res.* **16**, 1039–1049 (2017).
161. Müller, T. et al. Automated sample Preparation with SP3 for low-input clinical proteomics. *Mol. Syst. Biol.* **16**, e9111 (2020).
162. Sielaff, M. et al. Evaluation of FASP, SP3, and iST protocols for proteomic sample Preparation in the low microgram range. *J. Proteome Res.* **16**, 4060–4072 (2017).
163. Moggridge, S., Sorensen, P. H., Morin, G. B. & Hughes, C. S. Extending the compatibility of the SP3 paramagnetic bead processing approach for proteomics. *J. Proteome Res.* **17**, 1730–1740 (2018).
164. Lampaki, D., Diepold, A., Glatter, T. A. & Serial Sample Processing strategy with improved performance for in-Depth quantitative analysis of type III secretion events in *Pseudomonas aeruginosa*. *J. Proteome Res.* **19**, 543–553 (2020).
165. Knecht, S., Eberl, H. C. & Bantscheff, M. Interval-Based secretomics unravels Acute-Phase response in hepatocyte model systems. *Mol. Cell. Proteom.* **21**, 100241 (2022).
166. HaileMariam, M. et al. S-Trap, an ultrafast Sample-Preparation approach for shotgun proteomics. *J. Proteome Res.* **17**, 2917–2924 (2018).
167. Laskar, D. D., Tucker, M. P., Chen, X., Helms, G. L. & Yang, B. Noble-metal catalyzed hydrodeoxygenation of biomass-derived lignin to aromatic hydrocarbons. *Green. Chem.* **16**, 897–910 (2014).
168. Nakamura, H. & Watano, S. Direct permeation of nanoparticles across cell membrane: A review. *KONA Powder Part. J.* **35**, 49–65 (2018).
169. Lipke, P. N. & Ovalle, R. Cell wall architecture in yeast: new structure and new challenges. *J. Bacteriol.* **180**, 3735–3740 (1998).
170. Lu, X., Zheng, X., Li, X. & Zhao, J. Adsorption and mechanism of cellulase enzymes onto lignin isolated from corn Stover pretreated with liquid hot water. *Biotechnol. Biofuels*. **9**, 118 (2016).
171. Ashengroph, M. & Amini, J. Bioconversion of isoeugenol to Vanillin and vanillic acid using the resting cells of *Trichosporon Asahii*. *3 Biotech.* **7**, 358 (2017).
172. Casey, J. & Dobb, R. Microbial routes to aromatic aldehydes. *Enzyme Microb. Technol.* **14**, 739–747 (1992).
173. Jia, S. R., Cui, J. D., Li, Y. & Sun, A. Y. Production of L-phenylalanine from *trans*-cinnamic acids by high-level expression of phenylalanine ammonia lyase gene from *Rhodosporidium toruloides* in *Escherichia coli*. *Biochem. Eng. J.* **42**, 193–197 (2008).
174. Adeboye, P. T., Bettiga, M. & Olsson, L. ALD5, PAD1, ATF1 and ATF2 facilitate the catabolism of coniferyl aldehyde, ferulic acid and *p*-coumaric acid in *Saccharomyces cerevisiae*. *Sci. Rep.* **7**, 42635 (2017).
175. Konzock, O., Zaghen, S. & Norbeck, J. Tolerance of *Yarrowia lipolytica* to inhibitors commonly found in lignocellulosic hydrolysates. *BMC Microbiol.* **21**, 77 (2021).
176. Iwasaki, Y. et al. Novel metabolic pathway for salicylate biodegradation via phenol in yeast trichosporon moniliiforme. *Biodegradation* **21**, 557–564 (2010).
177. Bartsch, S. & Bornscheuer, U. T. Mutational analysis of phenylalanine ammonia lyase to improve reactions rates for various substrates. *Protein Eng. Des. Sel.* **23**, 929–933 (2010).
178. Konzock, O., Tous-Mohedano, M., Cibin, I., Chen, Y. & Norbeck, J. Cinnamic acid and *p*-coumaric acid are metabolized to 4-hydroxybenzoic acid by *Yarrowia lipolytica*. *AMB Express*. **13**, 84 (2023).
179. Lubbers, R. J. M. et al. A comparison between the homocyclic aromatic metabolic pathways from plant-derived compounds by bacteria and fungi. *Biotechnol. Adv.* **37**, 107396 (2019).
180. Mikkilä, J. et al. Fungal treatment modifies kraft lignin for lignin- and Cellulose-Based carbon fiber precursors. *ACS Omega*. **5**, 6130–6140 (2020).
181. Ravi, K., García-Hidalgo, J., Gorwa-Grauslund, M. F. & Lidén, G. Conversion of lignin model compounds by *Pseudomonas Putida* KT2440 and isolates from compost. *Appl. Microbiol. Biotechnol.* **101**, 5059–5070 (2017).
182. Falconnier, B. et al. Vanillin as a product of ferulic acid biotransformation by the white-rot fungus *Pycnoporus cinnabarinus* I-937: identification of metabolic pathways. *J. Biotechnol.* **37**, 123–132 (1994).
183. Guiraud, P., Steiman, R., Seigle-Murandi, F. & Benoit-Guyod, J. L. Metabolism of vanillic acid by micromycetes. *World J. Microbiol. Biotechnol.* **8**, 270–275 (1992).
184. Ander, P., Hatakka, A. & Eriksson, K. E. Vanillic acid metabolism by the White-Rot fungus *Sporotriehum pulverulentum*. *Arch. Microbiol.* **125**, 189–202 (1980).
185. Lubbers, R. J. M. et al. Discovery and functional analysis of a Salicylic acid hydroxylase from *Aspergillus Niger*. *Appl. Environ. Microbiol.* **87**, e02701–e02720 (2021).

186. The UniProt Consortium. UniProt: the universal protein knowledgebase in 2021. *Nucleic Acids Res.* **49**, D480–D489 (2021).
187. Yang, R. Y. et al. Genome sequence of the *Trichosporon Asahii* environmental strain CBS 8904. *Eukaryot. Cell.* **11**, 1586–1587 (2012).
188. Nordlund, I. & Shingler, V. Nucleotide sequences of the *meta*-cleavage pathway enzymes 2-hydroxymuconic semialdehyde dehydrogenase and 2-hydroxymuconic semialdehyde hydrolase from *Pseudomonas* CF600. *Biochim. Biophys. Acta BBA - Gene Struct. Expr.* **1049**, 227–230 (1990).
189. Inoue, J., Shaw, J. P., Rekik, M. & Harayama, S. Overlapping substrate specificities of benzaldehyde dehydrogenase (the XylC gene product) and 2-hydroxymuconic semialdehyde dehydrogenase (the XylG gene product) encoded by TOL plasmid pWW0 of *Pseudomonas Putida*. *J. Bacteriol.* **177**, 1196–1201 (1995).
190. Kato, H. et al. Identification and characterization of methoxy- and dimethoxyhydroquinone 1,2-dioxygenase from *Phanerochaete Chrysosporium*. *Appl. Environ. Microbiol.* **90**, e01753–e01723 (2024).
191. O'Fallon, J. V., Busboom, J. R., Nelson, M. L. & Gaskins, C. T. A direct method for fatty acid Methyl ester synthesis: application to wet meat tissues, oils, and feedstuffs. *J. Anim. Sci.* **85**, 1511–1521 (2007).
192. Xie, S., Sun, S. & Dai, S. Y. Efficient coagulation of microalgae in cultures with filamentous fungi. *Algal Res.* **2**, 28–33 (2013).
193. Li, X. et al. Discovery of potential pathways for biological conversion of Poplar wood into lipids by co-fermentation of *Rhodococci* strains. *Biotechnol. Biofuels*. **12**, 60 (2019).
194. Schneider, C. A., Rasband, W. S. & Eliceiri, K. W. NIH image to imageJ: 25 years of image analysis. *Nat. Methods*. **9**, 671–675 (2012).
195. Gluth, A. et al. Integrative Multi-PTM proteomics reveals dynamic Global, Redox, Phosphorylation, and acetylation regulation in Cytokine-Treated pancreatic beta cells. *Mol. Cell. Proteom.* **23**, 100881 (2024).
196. Xu, Z. et al. Understanding of bacterial lignin extracellular degradation mechanisms by *Pseudomonas Putida* KT2440 via secretomic analysis. *Biotechnol. Biofuels Bioprod.* **15**, 117 (2022).
197. Ritchie, M. E. et al. Limma powers differential expression analyses for RNA-sequencing and microarray studies. *Nucleic Acids Res.* **43**, e47 (2015).
198. Kanehisa, M., Sato, Y., Kawashima, M., Furumichi, M. & Tanabe, M. KEGG as a reference resource for gene and protein annotation. *Nucleic Acids Res.* **44**, D457–D462 (2016).
199. Kanehisa, M. & Goto, S. KEGG: Kyoto encyclopedia of genes and genomes. *Nucleic Acids Res.* **28**, 27–30 (2000).
200. Wu, T. et al. ClusterProfiler 4.0: A universal enrichment tool for interpreting omics data. *The Innovation* **2**, 100141 (2021).
201. Wickham, H. *ggplot2: Elegant Graphics for Data Analysis* (Springer-, 2016).

Acknowledgements

We acknowledge the U.S. Department of Energy (DOE) Office of Energy Efficiency & Renewable Energy (DE-EE0008250, and DE-EE0009763), the U.S. Department of Agriculture (USDA) National Institute of Food and Agriculture (Hatch/Multi State project 1017904), and the Bioproducts, Science and Engineering Laboratory, Department of Biological Systems Engineering at Washington State University (WSU). Portions of this research were also supported by the Predictive Phenomics Initiative (TZ) conducted under the Laboratory Directed Research and Development Program at Pacific Northwest National Laboratory (PNNL) in addition to a project award from the Environmental Molecular Sciences Laboratory, a DOE Office of Science User Facility sponsored by the Biological and Environmental Research program under Contract No. DE-AC05-76RL01830. YP and AJR acknowledge partial support from the Center for Bioenergy Innovation (CBI) at Oak Ridge National Laboratory, a U.S. DOE Bioenergy Research Center supported by the Office of Biological and Environmental Research in the DOE Office of Science. AG is grateful for support from the PNNL-WSU Distinguished Graduate Research Program Fellowship. We are also thankful for the FAMEs protocol from PNNL scientists Mark G. Butcher and Angela M. Melville.

Author contributions

A.G. and B.Y. designed research; A.G., Y.P., D.H., and X.L. performed research; Y.P., D.H., X.C., A.J.R., T.Z., and W-J.Q. contributed new reagents/analytical tools; A.G., Y.P., D.H., and Z.J. analyzed data; A.G. wrote the original draft; B,Y. and W-J.Q. assisted with conceptualization, supervision, and acquisition of experimental resources and project funding. All authors contributed to manuscript revision.

Funding

The author(s) declare funding support was received for the research, authorship, and/or publication of this article. We acknowledge the U.S. Department of Energy (DOE) Office of Energy Efficiency & Renewable Energy (DE-EE0008250, and DE-EE0009763), the U.S. Department of Agriculture (USDA) National Institute of Food and Agriculture (Hatch/Multi State project 1017904), and the Bioproducts, Science and Engineering Laboratory, Department of Biological Systems Engineering at Washington State University (WSU). Portions of this research were also supported by the Predictive Phenomics Initiative (TZ) conducted under the Laboratory Directed Research and Development Program at Pacific Northwest National Laboratory (PNNL) in addition to a project award from the Environmental Molecular Sciences Laboratory, a DOE Office of Science User Facility sponsored by the Biological and Environmental Research program under Contract No. DE-AC05-76RL01830. The views and opinions of the authors expressed herein do not necessarily state or reflect those of the United States Government or any agency thereof. Neither the United States Government nor any agency thereof, nor any of their employees, makes any warranty, expressed or implied, or assumes any legal liability or responsibility for the accuracy, completeness, or usefulness of any information, apparatus, product, or process disclosed, or represents that its use would not infringe privately owned rights.

Declarations

Competing interests

The authors declare no competing interests.

Additional information

Supplementary Information The online version contains supplementary material available at https://doi.org/10.1038/s41598-026-36483-5.

Correspondence and requests for materials should be addressed to B.Y.

Reprints and permissions information is available at www.nature.com/reprints.

Publisher's note Springer Nature remains neutral with regard to jurisdictional claims in published maps and institutional affiliations.